

# Low-energy ion outflow from the sub-auroral region

Tony T. Giang

IRF Scientific Report 300

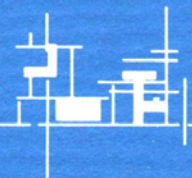
January 2010

ISSN 0284-1703

ISBN 978-91-977255-6-9

**INSTITUTET FÖR RYMDFYSIK**  
**Swedish Institute of Space Physics**

Umeå, Sweden





# Low-energy ion outflow from the sub-auroral region

by

**Tony T. Giang**

Swedish Institute of Space Physics  
Teknikhuset  
SE-901 87 Umeå  
Sweden

Licentiate Thesis in Space Physics  
IRF Scientific Report 300  
January 2010

ISSN 0284-1703  
ISBN 978-91-977255-6-9

LICENTIATE THESIS AT THE SWEDISH INSTITUTE OF SPACE PHYSICS  
Low-energy ion outflow from the sub-auroral region

Copyright © 2010 by Tony T. Giang  
IRF Scientific Report 300  
ISSN: 0284-1703  
ISBN: 978-91-977255-6-9  
Printed by: Universitetservice US-AB  
Stockholm, Sweden 2010

## **Abstract**

The magnetosphere is a magnetic cavity in space that results from the solar wind's interaction with the Earth's dipole magnetic field. The Earth's magnetic field acts as an effective shield against the solar wind. Only a minor fraction of the solar wind plasma has access to the magnetosphere. The magnetosphere consists of different regions with plasma of planetary and solar wind origin. The contributions from the solar wind plasma and the planetary plasma, the latter produced by outflow from the high-latitude ionosphere, into the magnetosphere have been the subject of thorough investigations for more than 30 years.

The focus in this thesis is on the planetary low-energy (40 – 200 eV) ion outflow from the sub-auroral regions (latitudes lower than the auroral oval) into the magnetosphere. Increased knowledge about the ion outflow is expected to enhance our knowledge about loss processes in the Earth's atmosphere. This thesis is about various factors that influence the sub-auroral low-energy ion outflow, such as the outflow for various magnetic disturbances. The results show that planetary low-energy ion outflow into the magnetosphere also occurs during magnetically quiet periods. The outflow of low-energy H<sup>+</sup>, He<sup>+</sup> and O<sup>+</sup> increases with increasing magnetic disturbance levels in the dawn, noon and dusk sectors, while for the midnight sector the low-latitude ion outflow appears to decrease with increasing magnetic disturbances. We argue that differences in the amount of ion outflow may be related to a supply from different ion sources. The ion outflow composition for the dawn, noon and dusk sectors seem to be the ionosphere and the plasmasphere. For the midnight sector the ion sources seem to be a combination of the nightside ionosphere and the dayside cleft ion fountain. Those two ion sources are known to be less dependent on geomagnetic activity. We have also estimated the total sub-auroral planetary low-energy ion outflow into the inner magnetosphere independently of the MLT:  $4.2 \cdot 10^{26} \text{ s}^{-1}$  for the H<sup>+</sup>,  $7.1 \cdot 10^{25} \text{ s}^{-1}$  for the He<sup>+</sup> and  $3.2 \cdot 10^{26} \text{ s}^{-1}$  for the O<sup>+</sup>.



## **List of included papers**

This thesis is based on the work reported in the following papers.

**Paper I**      **T. T. Giang**, M. Hamrin, M. Yamauchi, R. Lundin, H. Nilsson, Y. Ebihara, H. Rème, I. Dandouras, C. Vallat, M. B. Bavassano-Cattaneo, B. Klecker, A. Korth, L. M. Kistler and M. McCarthy  
**Outflowing protons and heavy ions as a source for the sub-keV ring current**  
*Annales Geophysicae*, Vol. 27, pages 839-849, 2009.

**Paper II**      **T. T. Giang**, M. Hamrin, R. Lundin, H. Rème and I. Dandouras  
**Low-energy ion outflow into the Earth's inner magnetosphere**  
Submitted for publication in *Annales Geophysicae*, June 2009.

Reprints were made with permission from the publisher.



# CONTENTS

<b>Introduction .....</b>	<b>1</b>
<b>The near-Earth space environment.....</b>	<b>3</b>
<b>Ion and electron motion in a magnetic dipole field .....</b>	<b>7</b>
Adiabatic invariants .....	10
The first adiabatic invariant .....	10
The second adiabatic invariant .....	11
The third adiabatic invariant .....	11
<b>The ionosphere .....</b>	<b>13</b>
<b>Space physics definitions .....</b>	<b>17</b>
<b>The ionosphere as a source for magnetospheric plasma .....</b>	<b>21</b>
<b>Plasma loss processes in the magnetosphere .....</b>	<b>23</b>
<b>Summary of papers.....</b>	<b>27</b>
Paper 1 .....	27
Paper 2.....	27
<b>Acknowledgements.....</b>	<b>29</b>
<b>Bibliography .....</b>	<b>31</b>
<b>List of acronyms .....</b>	<b>35</b>



# Chapter 1

## INTRODUCTION

The Sun is the major energy source for life in our solar system. The Sun and space have fascinated humans as long as we have existed on the Earth. Space phenomena have always been interpreted differently in different cultures. We know this from cave paintings made by our ancestors where they tried to describe space phenomena. Some religious beliefs seem to interpret celestial phenomena as signs from the gods.

Today we know that the phenomena in the sky may involve interactions between the solar wind (plasma from the corona of the Sun) and the Earth. To be able to understand the physics in space and solar wind plasma processes, we have to understand the basic physics of plasmas. This can be done with experiments in physics laboratories, with theoretical studies or with *in-situ* plasma measurements in space, that is by measurements made by instruments in space. Using *in-situ* instruments, the near-Earth space environment seems to be the best place to study and understand the solar wind, plasma processes and space physics. This is what solar-terrestrial physics is about, to study and understand the basic space plasma physics in the solar-terrestrial environment. An interesting aspect of solar-terrestrial physics is the outflow of planetary ions. The planetary ion outflow has direct influence on the atmosphere, which is so important for life on Earth.



## Chapter 2

### THE NEAR-EARTH SPACE ENVIRONMENT

Plasma is the dominating state of visual matter in the Universe. Of the known matter in the Universe, 99% is in the plasma state, e.g., nebulae, stars and the interstellar medium. Plasma can be described as an ionized gas where the atoms are dissociated into positive ions and negative electrons (Chen, 1984). The stars, including the Sun, are composed of dense plasmas while the interplanetary space mainly consists of tenuous plasmas. The solar wind is the kind of tenuous plasma that fills the interplanetary medium. Electric and magnetic fields interact with charged particles in the plasma and affect the behaviour and motion of the plasma.

The solar wind affects and interacts with all planets and bodies in our solar system. For magnetized bodies such as the Earth, the interaction between the planetary magnetic dipole field and the solar wind results in the formation of a magnetic cavity, a magnetosphere, around the planet. The magnetosphere acts as a shield against the solar wind. For life on Earth, this shielding against energetic particles is essential. The shape of the magnetosphere is compressed in the sunward direction (dayside), a compression caused by the kinetic pressure of the solar wind, and it is extended in the anti-sunward direction (nightside), similar to the tail of a comet. For unmagnetized bodies, an induced magnetosphere is also formed as a result of the solar wind interaction (Parks, 2004). The magnetosphere consists of various plasma regions, see Figure 1.

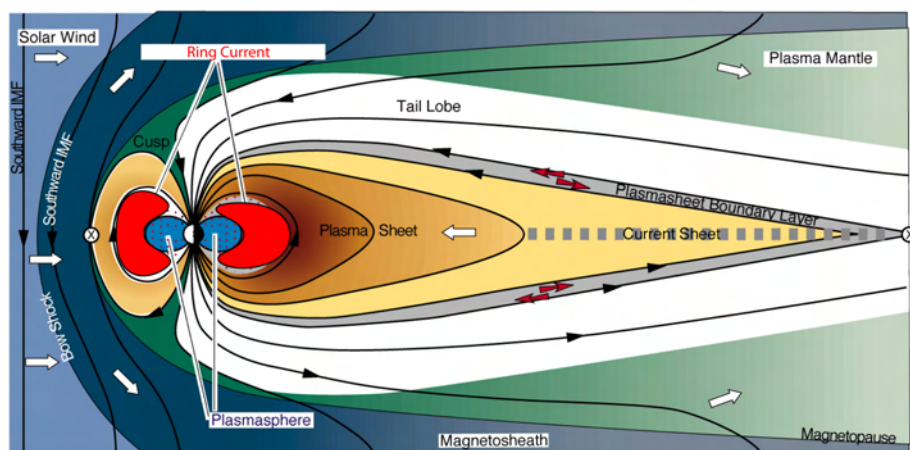


Figure 1: The Earth's magnetosphere and its plasma structures. From [http://www.igpp.ucla.edu/public/THEMIS/SCI/Pubs/Nuggets/PS\\_ring\\_current/Penetration%20of%20plasma%20sheet.HTML](http://www.igpp.ucla.edu/public/THEMIS/SCI/Pubs/Nuggets/PS_ring_current/Penetration%20of%20plasma%20sheet.HTML). Courtesy of P. H. Reiff, Physics and Astronomy Department, Rice University.

The bow shock is the boundary where the supersonic solar wind slows down to subsonic speeds and deflects around the Earth within the magnetosheath. The magnetosheath is located between the bow shock and the magnetopause. The magnetopause is the outer border of the Earth's magnetic field and it shields the magnetosphere from the shocked solar wind. It is difficult for the solar wind to penetrate into the magnetosphere. The magnetopause is usually located at about 10 Earth radii ( $R_E$ ) from the center of the Earth. On the dayside, the location varies due to its dependences on the solar wind dynamic pressure and on the strength of the magnetic field. The magnetopause is important because it is here the coupling between the solar wind and the magnetosphere occurs. At the magnetopause the pressure of the solar wind and the magnetic pressure of the Earth's geomagnetic field are in approximate equilibrium:

$$\rho_{SW} v_{SW}^2 = \frac{B_M^2}{2\mu_0} \quad (1)$$

where  $\rho_{SW}$  and  $v_{SW}$  represent the plasma mass density and the solar wind velocity.  $B_M$  and  $\mu_0$  are the magnetospheric magnetic field and the permeability of free space. On the nightside, the magnetopause extends to distances of hundreds of  $R_E$ . Despite the shielding by the magnetopause against the entry of the solar wind plasma into the magnetosphere, some solar wind plasma can still find its way through the dayside magnetopause. The solar wind plasma entrance through the dayside magnetopause involves for example direct transfer of plasma perpendicular to the geomagnetic field and also the reconnection process of the interplanetary magnetic field (IMF) and the geomagnetic field (Dungey, 1961). Solar wind plasma can also enter the magnetosphere on locally open region called the cusp (Burch, 1968). The cusp is located at the polar regions where the geomagnetic field lines are open to solar wind plasma entry (see Figure 1).

By the inner magnetosphere, we mean the sub-auroral part of the plasma sheet (latitudes lower than the auroral oval region), the plasmasphere and the radiation belts. The plasma in the inner magnetosphere consists of solar wind- and ionospheric particles.

The plasma sheet is located at the center of the magnetotail and it consists of a hot and low-density plasma. Plasma in the plasma sheet is a mixture of ions and electrons from the solar wind and accelerated particles from the ionosphere. The plasma sheet is an important source for the inner magnetosphere. During magnetic substorms and storms (see section 5) plasma sheet plasma will be injected Earthward into the plasmasphere and ring current region and supply these regions with plasma.

The plasmasphere constitutes the innermost region of the inner magnetosphere. The plasmasphere consists of cold and dense plasma, an extension of the Earth's low-latitude ionosphere. The plasmasphere is co-

rotating with the Earth. Further out, energetic ions are drifting westward and electrons are drifting eastward around the Earth due to a combination of the gradient-curvature drift and the  $\mathbf{E} \times \mathbf{B}$ -drift as described in later sections.

The auroral ovals are located with their centres around the geomagnetic poles, see Figure 2. The auroral oval was first identified with ground-based optical instruments (Fel'dshteyn, 1963). Solar activity has an effect on the latitudes of the ovals and shifts the ovals equatorward during enhanced solar activity.

The aurora is a consequence of charged particles from the magnetosphere precipitating into the Earth's atmosphere. Particle detectors onboard sounding rockets made the first measurements of the particles responsible for the aurora (e.g., Meredith *et al.*, 1958; McIlwain, 1960 and Davis *et al.*, 1960). The quality of particle detectors, e.g., onboard Viking and Freja, and quantity of data has increased over the years. A large number of statistical studies on particle precipitation have been presented, such as that by Hardy *et al.* (1985). The data have provided essential information about precipitating particles and their relationship with electromagnetic fields and waves in the magnetospheric plasma.

However, the auroral regions are not only connected with precipitating particles but are also associated with outflowing ionospheric ions. The S3-3 satellite discovered energetic ( $\approx 10$  eV – 10 keV) ionospheric ion outflow in the auroral region (e.g., Shelley *et al.*, 1976 and Chappell, 1988). *In-situ* measurements (e.g., Dynamics Explorer and Viking) showed the presence of different energization processes such as electrostatic field accelerations and field-aligned wave energizations in the high-altitude region (see e.g., Paschmann *et al.*, 2002 for a review). In fact, the physical processes leading to particle energization in the auroral region will not only lead to intense auroral phenomena, they will also lead to intense planetary plasma outflow.

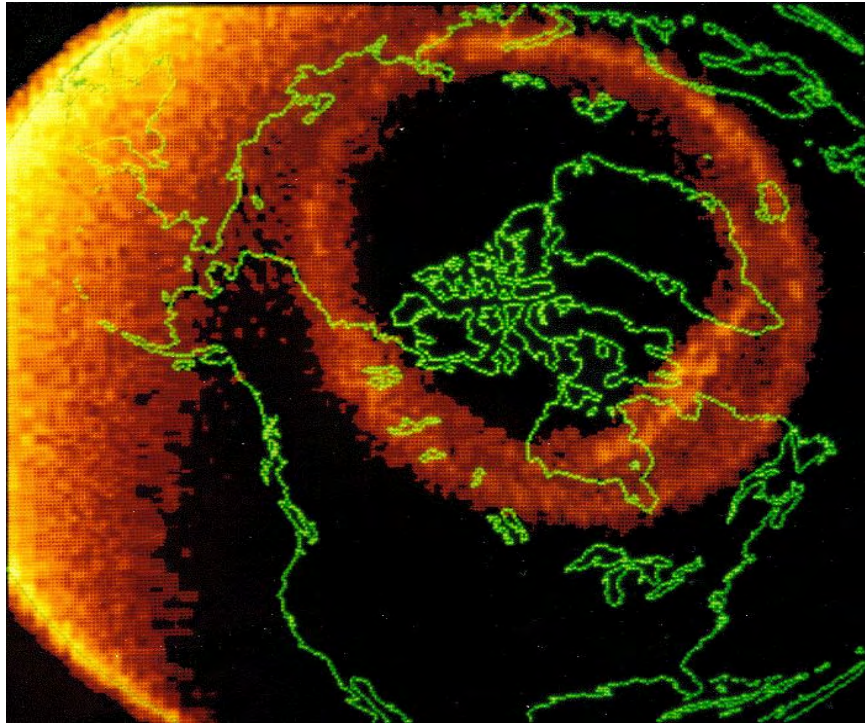


Figure 2: Image of the auroral oval with centre around the geomagnetic pole. The oval is located on the nightside of the magnetosphere, the dayside is located on the left side in the image. From <http://www-istp.gsfc.nasa.gov/istp/outreach/workshop/bobwhere.html>.

## Chapter 3

### ION AND ELECTRON MOTION IN A MAGNETIC DIPOLE FIELD

The magnetosphere constitutes an environment of magnetized plasma whose behaviour is determined by magnetic and electric forces. The following sections will briefly describe the basic features that determine the motion of a charged particle in magnetic and electric fields. More detailed descriptions can be found in various plasma and space physics textbooks, (e.g., Roederer, 1970; Chen, 1984; Kivelson and Russel, 1995; Fälthammar, 2001 and Parks, 2004).

The plasma is assumed to be collisionless, i.e. the mean free path (the average distance covered by a particle between collisions) of the particles is larger than the scale size of the system. A charged particle  $q$ , with velocity  $\mathbf{v}$ , will in a magnetic field  $\mathbf{B}$  experience a force  $\mathbf{F}$ , called the Lorentz force:

$$\mathbf{F} = q\mathbf{v} \times \mathbf{B}. \quad (2)$$

The Lorentz force acting on a particle can be written as a centripetal force  $F_C$ :

$$F_C = \frac{mv_{\perp}^2}{r} \quad (3)$$

where  $m$  is the mass of the particle,  $v_{\perp}$  is the particle velocity component perpendicular to the magnetic field and  $r$  is the distance from the particle to its guiding center (radius of curvature). Combining equations 2 and 3 leads to:

$$r_L = \frac{mv_{\perp}}{|q|B} \quad (4)$$

which is the definition of the Larmor radius. The result of the Lorentz force is therefore that a particle will gyrate around a magnetic field line at a distance given by the Larmor radius.

From the Larmor radius one may derive the gyro frequency  $f$ , (also called the cyclotron frequency):

$$f = \frac{v_{\perp}}{2\pi r_L} = \frac{|q|B}{2\pi m}. \quad (5)$$

From equations (1), (3) and (4) we see that ions and electrons behave differently due to their different masses and charges. The Lorentz force causes the ions and electrons to gyrate in opposite directions. Ions have larger Larmor radii and lower gyro frequencies than electrons due to their larger masses.

A charged particle in a diverging (dipole) magnetic field  $\mathbf{B}$  without the influence of external forces will gyrate around the magnetic field line with perpendicular velocity  $v_{\perp}$  and parallel velocity  $v_{\parallel}$ . During the motion in the magnetic field, the total kinetic energy  $W_k$  is preserved, and the charged particle kinetic energy is distributed between a parallel  $W_{\parallel}$  and a perpendicular  $W_{\perp}$  component such that  $W_k = W_{\parallel} + W_{\perp}$ . Hence, if  $v_{\parallel}^2$  decreases then  $v_{\perp}^2$  increases and vice versa to keep the total kinetic energy constant.

The pitch-angle  $\alpha$  is defined as the angle between the velocity vector  $\mathbf{v}$  and the magnetic field  $\mathbf{B}$ , i.e.  $\alpha = \arcsin \frac{v_{\perp}}{v}$ , where  $v_{\perp}$  is the velocity component perpendicular to  $\mathbf{B}$ , see Figure 3. At magnetic mirror points, i.e. for  $\alpha = 90^\circ$  all particle kinetic energy will be in form of  $v_{\perp}$ , ( $\mathbf{v} = v_{\perp}$ ), i.e.  $W_k = W_{\perp} = \frac{mv_{\perp}^2}{2}$ , for non-relativistic motion. Particles, for example ions, which experience a mirror force in a dipole magnetic field will bounce between the mirror points (see also the second invariant on page 11).

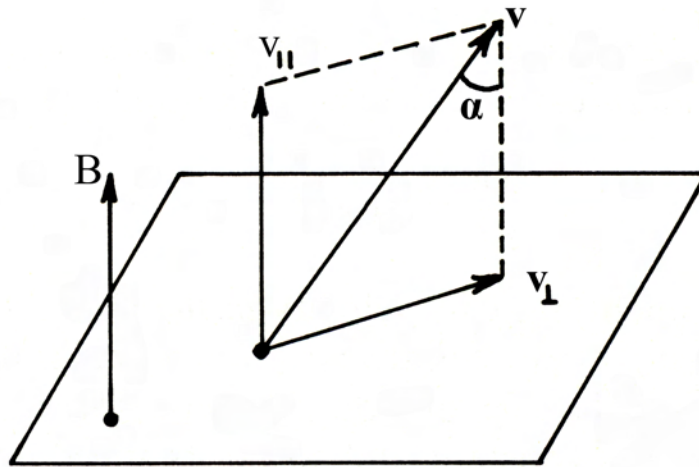


Figure 3: Schematic illustration of a charged particle motion in a magnetic field without influences of external forces. The angle  $\alpha$ , between the particle velocity vector  $\mathbf{v}$  and the magnetic field  $\mathbf{B}$ , is the pitch-angle. After Roederer, 1970.

The loss cone is a cone that separates mirroring from precipitating charged particles. Charged particles inside the loss cone will interact with the Earth's atmosphere and become "lost". The lost particles provide energy and

mass to the atmosphere, while particles outside the loss cone will be reflected by the magnetic mirror force and bounce between magnetic mirror points (Figure 6). The loss cone angle is defined as

$$\alpha_{\text{loss cone}} = 2 \arcsin \sqrt{B/B_{\text{max}}} \quad (6)$$

where  $B$  is the magnetic field strength and  $B_{\text{max}}$  is the maximum magnetic field strength at the magnetic mirror point.

A charged particle  $q$ , in an electric field  $\mathbf{E}$ , will also experience an electric force  $\mathbf{F}$ , given by

$$\mathbf{F} = q\mathbf{E}. \quad (7)$$

A charged particle in an electric field perpendicular to the magnetic field will drift perpendicular to both the magnetic and electric fields. This particle-drift is the  $\mathbf{E} \times \mathbf{B}$ -drift and it is given by

$$\mathbf{v} = \frac{\mathbf{E} \times \mathbf{B}}{B^2}. \quad (8)$$

The  $\mathbf{E} \times \mathbf{B}$ -drift is energy- and charge independent, i.e. ions and electrons will drift in the same direction. If the magnetic field is inhomogeneous, i.e. magnetic gradients are present, there will also be a gradient drift ( $\nabla B$ -drift). The  $\nabla B$ -drift is given by

$$\mathbf{V} = \frac{-\square}{q} (\nabla B) \times \frac{\mathbf{B}}{B^2}; \quad \square = \frac{mv_{\perp}^2}{2B}. \quad (9)$$

The  $\nabla B$ -drift is caused by changes of the Larmor radius in an inhomogeneous magnetic field according to equation (4). The  $\nabla B$ -drift is energy- and charge dependent, i.e. ions and electrons drift in opposite directions.

A curved magnetic field will cause a curvature drift according to

$$v = \frac{mv_{\perp}^2}{RqB} \quad (10)$$

where  $R$  is the radius of curvature of the magnetic field. From equation (10) one can see that the curvature drift is energy- and charge dependent. The three particle drift motions are illustrated in Figure 4.

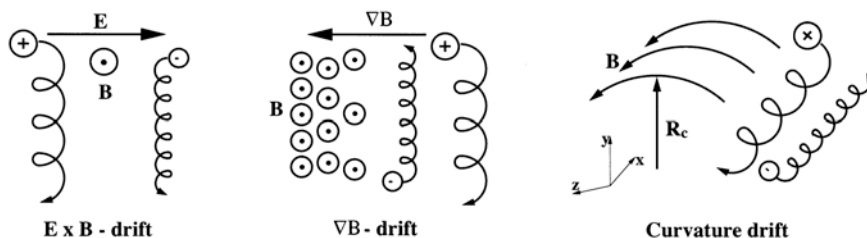


Figure 4: Illustration of three drift motions for charged particles. From Høymark, 2001.

If we assume that the spatial and temporal changes of the magnetic field are very small compared to the Larmor radius (equation 4) and the gyro frequency (equation 5), and combining the three particle drift motions, (equations 8, 9 and 10) we can derive three adiabatic invariants, i.e. invariants describing the conservations of total energy and magnetic moment of charged particles. Figure 5 illustrates the particle motions governed by three adiabatic invariants.

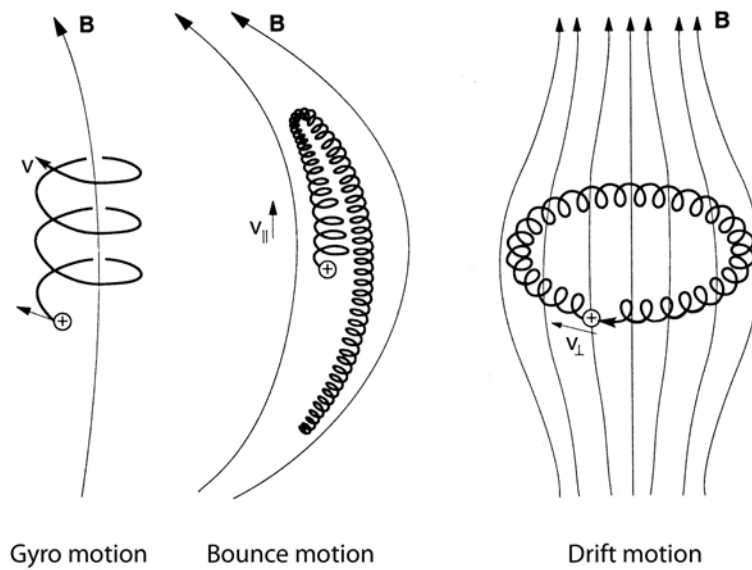


Figure 5: Schematic illustration of the particle motions corresponding to the three adiabatic invariants. After Fälthammar, 2001.

### Adiabatic invariants

“An adiabatic invariant is a property of a physical system which stays constant when changes are made slowly.” – Definition retrieved from Wikipedia.

In space plasma physics this applies to, for instance, the particle motion in a dipole magnetic field, as described in the previous section. The three adiabatic invariants described here require that the changes in energy and momentum are small during gyro-, bounce- and drift motion.

### *The first adiabatic invariant*

A circular current will occur when charged particles are gyrating around a magnetic field line. The current will have a magnetic moment directed

opposite to the magnetic field. The magnitude of the magnetic moment is the product of the average current ( $I = fq$ ) and the area enclosed by the gyro circle ( $A = \pi r_L^2$ ), i.e.:

$$\square = \frac{|q|B}{2\pi m} q\pi \left[ \frac{mv_{\perp}}{|q|B} \right]^2 = \frac{mv_{\perp}^2}{2B} \quad (11)$$

where  $m$  and  $v_{\perp}$  are the mass and perpendicular velocity of the particle in the magnetic field  $\mathbf{B}$ . The magnetic moment  $\square$ , is independent of time and is constant in the guiding centre motion if the variations of the magnetic field are small compared to the Larmor radius (equation 4) and the gyro frequency (equation 5). The first adiabatic invariant is given by equation 11.

### ***The second adiabatic invariant***

A charged particle with a certain kinetic energy will, besides the gyration around the magnetic field line, also travel along the field line. The particle will travel along the field line until its parallel velocity ( $v_{\parallel}$ ) is zero, then all the kinetic energy will be in the form of perpendicular velocity ( $v_{\perp}$ ), see Figure 5. The location where  $v_{\parallel}$  is zero is called the mirror point, see Figure 6. The longitudinal oscillation (the bounce period between the mirror points) is constant if the change of the magnetic mirror field is very small during each individual longitudinal oscillation period. The second adiabatic invariant is given by

$$J = \int_{s_1}^{s_2} mv_{\parallel} ds = \text{constant} \quad (12)$$

where  $m$  is the mass of the particle,  $s_1$  and  $s_2$  are the magnetic mirror points and  $v_{\parallel}$  is the parallel velocity of the particle in the magnetic field  $\mathbf{B}$ .

### ***The third adiabatic invariant***

The magnetic flux  $\Phi$ , enclosing the guiding drift shell, a surface generated by the particle guiding centre during the drifts of a particle, is constant if the changes of the dipole field are slow compared to the drift period, see Figure 5. The third adiabatic invariant is given by

$$\Phi = \int \mathbf{A}_0 \cdot d\mathbf{x} = \text{constant} \quad (13)$$

where  $\mathbf{A}_0$  is the magnetic vector potential (Roederer, 1970). Equation (13) describes a constant magnetic flux if a particle is drifting on constant magnetic vector potential (similar to drift shell). Figure 6 illustrates a trapped particle drift under the conditions of the three adiabatic invariants. The charged particle will gyrate around the magnetic field line and bounce between two mirror points. At the same time, the trapped particle will drift around the Earth on the same drift shell and enclose constant magnetic flux during the drift. Depending on the particle charge, the drift will have different directions for ions and electrons; ions drifting westwards and

electrons drifting eastwards according to equations 9 and 10. However, for small perpendicular velocities  $v_{\perp}$ , the gradient-curvature drift (equation 9 and 10) may be superseded by the  $\mathbf{E} \times \mathbf{B}$ -drift (equation 8). This is for example, the case for low-energy ions in the plasmasphere.

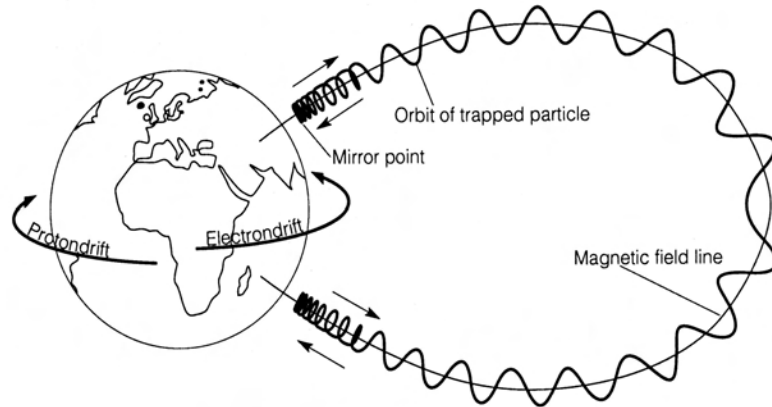


Figure 6: Illustration of the three basic motions of charged trapped particles in the geomagnetic field: gyro, bounce between mirror points, and drift. From Fälthammar, 2001.

The ring current region is located in the inner magnetosphere between  $2 - 7 R_E$ . The ring current in the Earth's dipole magnetic field is a consequence of charged particles drift in plasma pressure gradients. The ions and electrons in the ring current experience both a gradient-curvature and  $\mathbf{E} \times \mathbf{B}$ -drift. The result of these combined drifts is energetic ions drifting westward, electrons and low-energy ions drifting eastward. Under certain boundary conditions, e.g., pressure gradients, this will give rise to a westward electrical current. The particles in the ring current will produce a magnetic field with the opposite direction compared to the Earth's geomagnetic field. This will result in a slightly decreased surface magnetic field in the equatorial region on Earth (Williams, 1983).

## Chapter 4

### THE IONOSPHERE

A layer of gas, the atmosphere, encompasses the Earth. The thickness of the atmosphere is about 1000 km and can be divided into different layers. The layers are, from the ground up, the troposphere, the stratosphere, the mesosphere, the thermosphere and the exosphere.

The upper part of the atmosphere between the neutral atmosphere and the magnetosphere, at approximately 80 - 1000 km altitudes, is called the ionosphere. A fraction of the gas in the ionosphere remains ionized due to solar Extreme Ultra-Violet (EUV) radiation and a low recombination rate. Recombination is a process where ions capture electrons and become neutral atoms or molecules. The maximum ionized particle density peaks at about 250 - 300 km altitude where the recombination rate is the lowest.

Since the ionosphere stems from ionization of atmospheric atoms and molecules it is of interest to describe the atmosphere in more detail. The atmospheric composition change with altitude is due to the decreasing temperatures with increasing altitude and depends on the scale height. In hydrostatic equilibrium the pressure ( $p$ ) force  $\left(\frac{-dp}{dz}\right)$  is balanced by the gravitational force ( $g\rho$ ), i.e.:

$$\frac{-dp}{dz} = g\rho \quad (14)$$

where  $g$  is the gravitational acceleration,  $\rho$  is the mass density of a volume element, where  $\rho = nM$ ;  $n$  is the number density of the gas,  $M$  is the mean molecular mass, and  $z$  is the altitude coordinate with positive sign upward. The ideal gas law is defined as:

$$p = nkT = \frac{\rho}{M}kT \quad (15)$$

Where  $k$  is the Boltzmann's constant ( $k = 1.38 \cdot 10^{-23}$  J/K) and  $T$  is the absolute temperature. If the temperature is constant and combining equations 14 and 15 will lead to:

$$\frac{-dp}{dz} = g\rho = g\left(\frac{pM}{kT}\right). \quad (16)$$

Equation 16 can be re-written as:

$$dp = -p\left(\frac{gM}{kT}\right)dz. \quad (17)$$

Integration of equation 17 leads to:

$$p = p_0 e^{\left(\frac{-gM}{kT}z\right)} = p_0 e^{\left(\frac{-z}{H}\right)}. \quad (18)$$

The scale height  $H$  is given by

$$H = \frac{kT}{Mg}. \quad (19)$$

In a similar manner the ionized gas will have a similar dependence on height as that of the atmosphere. One may therefore assume that the ion stratifications in the ionosphere have similar features to those in the atmosphere.

Equation (19) shows that the scale height remains constant if the temperature and mean molecular mass do not vary and this explains the ionospheric ion composition and layering at different altitudes (temperatures). However, ion species with different mean molecular mass ( $M$ ) will have different scale heights at the same temperature. For the atmosphere on Earth, the ion species are stratified as illustrated in Figure 7. At about 900 km altitude there is a cross-over where  $H^+$  ions start to be the dominant ion species. The domination of  $H^+$  ions at altitudes higher than 900 km is due to its lighter atomic mass compared to for instance  $He^+$  and  $O^+$  ions.

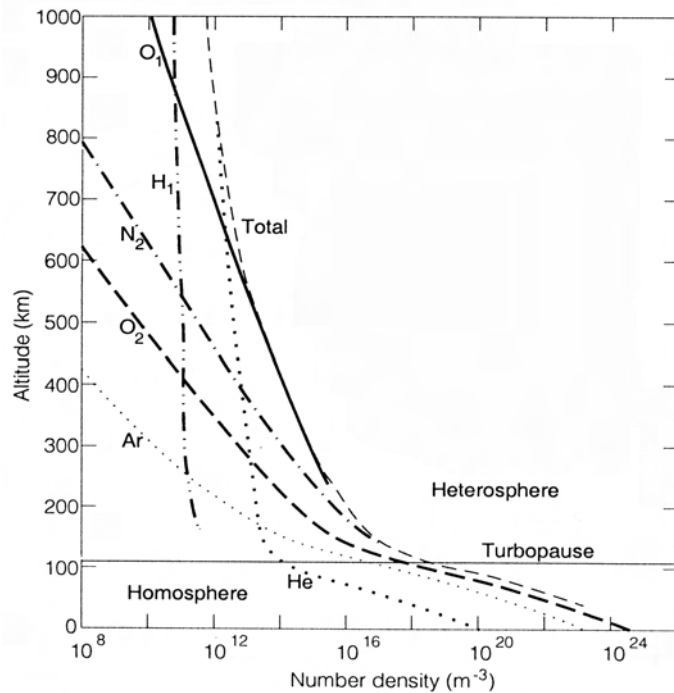


Figure 7: The ion stratifications at different altitudes of the Earth's atmosphere. The  $H^+$  ions dominate at altitudes higher than 900 km due to their lighter atomic mass. From Fälthammar, 2001.

In the *D* and *E* layers, the dominant ion species are primarily the heavier positive ions, e.g.,  $\text{NO}^+$ ,  $\text{O}_2^+$ , while the dominant ion species in the *F*-layers ( $F_1$  and  $F_2$ ) is  $\text{O}^+$ , see Table 1.

At lower latitudes, at about 1500 km altitude, the ionosphere will gradually merge into a plasma region called the plasmasphere. Together with the ionosphere, the plasmasphere is the nearest magnetospheric plasma population to the Earth and consists of a dense and cold plasma. The plasmaspheric plasma is formed by diffusion of ions from plasma regions in the ionosphere. The dominant ion species in the plasmasphere are lighter ions such as  $\text{H}^+$  and  $\text{He}^+$ .

Layer	<i>D</i>	<i>E</i>	$F_1$	$F_2$
Altitude [km]	60 – 85	85 – 140	140 – 200	200 – ca 1500
Nighttime electron density [m <sup>-3</sup> ]	$< 10^8$	$2 \cdot 10^9$	----	$(2-5) \cdot 10^{11}$
Daytime electron density [m <sup>-3</sup> ]	$10^9$	$(1-2) \cdot 10^{11}$	$(2-5) \cdot 10^{11}$	$(0.5-2) \cdot 10^{12}$
Ion species	$\text{NO}^+$ , $\text{O}_2^+$	$\text{NO}^+$ , $\text{O}_2^+$	$\text{NO}^+$ , $\text{O}_2^+$ , $\text{O}^+$	$\text{H}^+$ , $\text{He}^+$ , $\text{O}^+$

Table 1: The ionospheric layers and their compositions. After Fälthammar, 2001.



## Chapter 5

### SPACE PHYSICS DEFINITIONS

Many different coordinate and time systems are used in space physics depending on the object or region that is in focus. In this thesis, the Geocentric Solar Magnetospheric coordinate system (GSM) and the Magnetic Local Time (MLT) are used to define the coordinates and time. The GSM system has the x-axis towards the Sun, the y-axis perpendicular to the magnetic field and the z-axis parallel to the magnetic northern pole. The MLT is a longitude (in hours) in the Earth's magnetic coordinate system.  $MLT = 12$  hours is the geomagnetic longitude that faces the Sun (magnetic noon), while  $MLT = 0$  is the magnetic midnight longitude that faces midnight (magnetic midnight).

The Earth's magnetic field is a dipole. However, in the outer region of the magnetosphere, currents induced by the solar wind perturb the dipole field. A departure from the classical dipole magnetic field therefore occurs, e.g., over the polar regions where the magnetic field lines are open and may connect to the IMF, see Figure 1. Geomagnetic field lines close to the Earth are connected to the geomagnetic poles at both ends, see Figures 1 and 8. Such field lines are denoted "closed field lines".

Geomagnetic indices are measurements of the variations in the geomagnetic field. These magnetic variations are induced by electric currents, for example electric currents in the ionosphere. Magnetic field data are collected at different observatories located at various places on Earth and transformed to different geomagnetic indices. Relevant geomagnetic indices for paper 1 and 2 in this thesis are described below.

The  $K$  index describes the disturbances in the horizontal component of the Earth's magnetic field. The disturbances are denoted with an integer in the range 0 - 9 with  $\leq 1$  being calm and  $\geq 5$  indicating strong geomagnetic disturbance.

The  $K_p$  index (which originates from *planetarische Kennziffer* and means planetary index) is derived as a weighted average of  $K$ -indices from 13 geomagnetic observatories located at sub-auroral latitudes. A high  $K_p$  index indicates disturbed geomagnetic conditions while a low  $K_p$  index indicates quiet conditions.

The  $D_{st}$  index (disturbance storm time index) is used to measure the severity of magnetic storms. The data is taken from observatories located at the equatorial region.

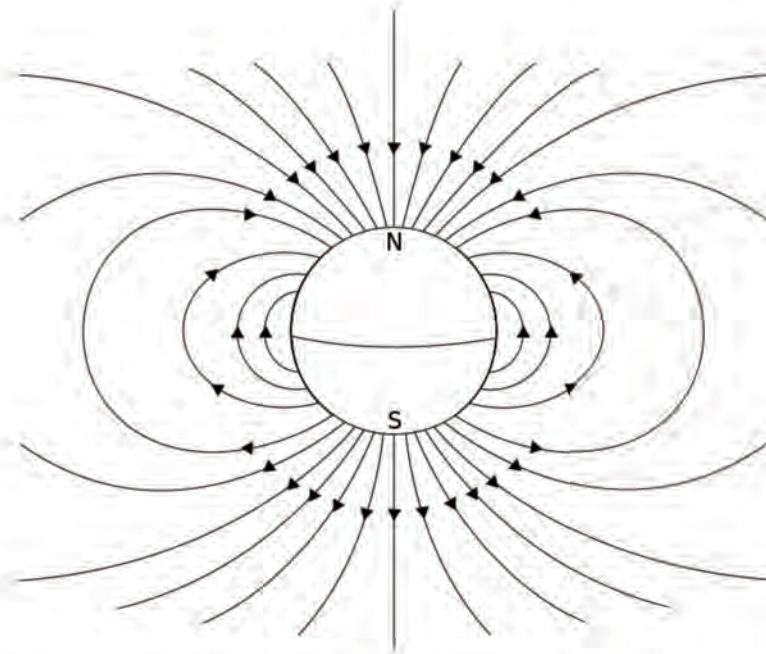


Figure 8: The geomagnetic dipolar field. Note that the “N” and “S” (north and south) refer to the geographic poles, while the magnetic poles are located in the opposite positions. (Dipole\_field.svg courtesy of the U.S. Geological Survey.)

Solar disturbances (e.g., corona mass ejections (CMEs) and coronal holes) lead to geomagnetic disturbances in the Earth’s magnetosphere, e.g., geomagnetic storms and magnetospheric substorms. Geomagnetic storms are major solar events associated with solar wind shock waves that compress the Earth’s magnetosphere. The effects of geomagnetic storms will last for a few days and will sometimes cause disruptions in communication systems and power networks on Earth. Geomagnetic disturbances are also related with enhanced ionospheric ion outflow.

Magnetic substorms are caused by solar wind driven energy releases in the magnetosphere, usually when the IMF turns southward, allowing interplanetary and terrestrial magnetic field lines to more easily merge in the dayside magnetosphere. During such disturbances, enhanced solar wind energy is transferred into the magnetosphere, leading for example to enhanced particle precipitations, intense aurora and enhanced electric currents in the magnetosphere. Magnetic substorms start in the magnetotail with a growth phase, followed by the expansion phase where the magnetic energy stored in the tail will energize charged particles in the plasma sheet

and inject particles into the inner magnetosphere. During the recovery phase, the magnetosphere gradually returns to a quiet state. Magnetospheric substorms last for about 2 – 3 hours, and auroras become intense and widespread in the polar regions.

The focus of this thesis is on magnetically quiet periods. I will demonstrate that ionospheric ion outflow, generally believed to be the characteristic of disturbed periods, also occurs during quiet periods.



## Chapter 6

### THE IONOSPHERE AS A SOURCE FOR MAGNETOSPHERIC PLASMA

The ionosphere is a major source of planetary ion outflow to the Earth's magnetosphere. The ionospheric outflow sources at high latitudes are located at different regions, e.g. auroral ion fountain, polar cap and cleft ion fountain, (e.g., Chappell, 1988). Ion energies and species in the outflow are different. This may be due to different energization processes in different regions.

Plasma can be energized by, for example, interactions with waves, the so-called wave-particle interaction process, or by parallel electric fields. The wave-particle interaction processes may contribute energy to the plasma in two ways, by increasing the thermal energy (heating) and/or by increasing the kinetic energy (acceleration). Wave-particle interactions may take place in the course of a particle gyration, bounce motion and drift motion, and hence violate one or more adiabatic invariants. The auroral ion fountain is characterized by outflow of energetic ionospheric ions (up to tens of keV), and it is related with enhanced solar wind – magnetosphere interaction. Enhanced  $O^+$  ion outflow is expected during strong solar activity (Chappell, 1988).

The polar cap is a region at auroral latitudes higher than the auroral oval latitudes. If looking down at the poles from space, the polar cap is a region void of auroral emissions enclosed by the auroral oval. The polar wind (Banks and Holzer, 1968) is a very low density, supersonic flux of cold, light ion outflow, from the polar cap into of the magnetospheric lobes. The polar wind has been observed at ionospheric topside heights by e.g., Brinton *et al.* (1971) and Hoffman *et al.* (1974). The composition of the polar wind is predominantly  $H^+$  and  $He^+$  ions with some  $O^+$  ion contribution. Energization of the ions in the polar cap is mainly due to ambipolar diffusion (positive and negative particles diffuse at the same rate due to their interaction via the electric field) and not to parallel acceleration processes as in the auroral oval. The energy of polar wind ions is typically a few electron volts (eV).

Upwelling ions from the so-called “cleft ion fountain” (Horwitz, 1987) are mostly observed in the morning sector of the auroral oval and at low latitudes of the dayside polar cap. The ion outflow is dominated by  $O^+$  ions, and this distinguishes it from the polar wind (dominated by  $H^+$  and  $He^+$  ions). The upwelling ions are energised in both the parallel and perpendicular direction up to tens of electron volts. The upwelling ions will

gradually become more field-aligned and reach higher altitudes. The upward (field-aligned) velocity is low compared to the horizontal convection velocity. The upwelling ions will spatially disperse across the polar cap toward the nightside. The cleft ion fountain is the dominating source of heavy ions in the polar cap magnetosphere (Horwitz, 1987). The cleft ion fountain is a plasma source also during geomagnetic quiet periods (low  $K_p$  indices).

The ion composition in the ionospheric  $F_2$ -layer makes it a conceivable source region for the outflow discussed above (see Table 1 in section 4).

The sub-auroral region is usually considered to be an almost unimportant region in terms of ion outflow. In this thesis I will present results implying that the sub-auroral region may contribute significantly to the outflow of planetary ions. The papers included in this thesis are focused on low-energy (40 – 200 eV) ion outflow from the sub-auroral region during different geomagnetic conditions.

## Chapter 7

### PLASMA LOSS PROCESSES IN THE MAGNETOSPHERE

The Earth's ionosphere and the solar wind are the main sources of plasma in the Earth's magnetosphere. Despite a constant supply of plasma, the magnetosphere is not overfilled by charged particles. This is because there are also plasma loss processes. On open magnetic field lines, charged particles will flow tailward, form the comet-like long geotail with particles that eventually will be lost to interplanetary space. However, some plasma may be injected back into the inner magnetosphere during geomagnetic disturbed conditions. Three different loss processes are mainly responsible for the plasma loss from the magnetosphere on closed, or semi-closed magnetic field lines: 1) particle drift, 2) particle precipitation and 3) charge exchange.

In section 3, it was pointed out that magnetospheric charged particles experience different kind of drifts ( $\mathbf{E} \times \mathbf{B}$ -drift,  $\nabla B$ -drift and curvature-drift) due to the  $\mathbf{E}$ - and  $\mathbf{B}$ -fields near the Earth. Charged particles drift around the Earth on different drift shells, either westward (ions) dominated by the  $\nabla B$ -drift and curvature-drift or eastward (electrons and low-energy ions) dominated by the  $\mathbf{E} \times \mathbf{B}$ -drift. The electric charge has a strong influence on the particle drift. Some of the drifting particles will be on drift shells (semi-closed field lines) that will intersect and cross the magnetopause on the dayside of the magnetosphere. Most of the drifting magnetospheric charged particles that cross the magnetopause will be lost into interplanetary space. *In-situ* measurements of the plasma of magnetospheric origin immediately outside the magnetopause demonstrates this (Meng and Anderson, 1970 and Hones *et al.*, 1972). Similar results were obtained by Sonnerup *et al.* (1981), Peterson *et al.* (1982) and Williams (1979) when they investigated the composition and spectra of the charged particles outside the dayside magnetopause.

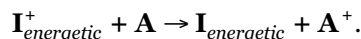
Satellite measurements during the 1960's showed that magnetospheric charged particles are precipitating into the Earth's atmosphere. Particles precipitating into the atmosphere are either scattered or forced into the loss cones, e.g. by waves. In regions with upward field-aligned currents, electrons may become accelerated downward by magnetic field-aligned electric fields, hence increasing the flux of magnetospheric electron precipitation. Hardy *et al.* (1985) found that the electron precipitation at high-latitudes is separated into two parts based on the electron average energy: 1) a region of hot

electrons ( $E_{AVE} \geq 600$  eV) where the electron average energies are highest on the morningside and 2) a region where the electron average energies are low ( $E_{AVE} < 600$  eV) and the largest number of fluxes are on the dayside.

Discrete aurora (the most intense type of aurora) is a consequence of enhanced electron precipitation into the atmosphere. Magnetic field-aligned electric fields is one mechanism causing such enhancements. Bingham *et al.* (1984) argued that the acceleration of auroral arc electrons is also the result of wave-particle acceleration, in particular by lower-hybrid waves. For other theories for enhanced electron precipitation see the review by Paschmann *et al.* (2002).

Waves can also cause pitch-angle scattering of protons and electrons in the equatorial region if their frequencies is of the order of their gyrofrequencies. Electromagnetic ion cyclotron (EMIC) waves in the equatorial plane reduce the perpendicular energy of the ions which leads to pitch-angle scattering and causes more precipitating particles to be scattered into the loss cone (Cornwall, 1965; Kozyra *et al.*, 1984 and Horne and Thorne, 1993).

Charge exchange is an interaction process between an energetic ion and a neutral atom or neutral molecule. The energetic ion changes its charge state by attracting an electron from the neutral atom or neutral molecule, see Figure 9. The charge exchange process will produce an energetic neutral atom (ENA),



The ENA is a fast moving neutral particle, retaining most of its original ion energy, see Bransden and McDowell (1992) for more details. The probability for a charge-exchange process is determined by the charge-exchange cross sections of the particles (Wurz, 2000). The charge exchange cross sections at low ion energies are within the range of  $10^{-15}$  cm<sup>2</sup> (Grigoriev, 2007). Unaffected by magnetic and electric forces, some ENAs may be lost into space when travelling along a straight, line-of-sight path from the point where it was created, see Figure 9, whereas others go into the atmosphere and represent a gain (Hultqvist *et al.*, 1999). The charge-exchange process between protons and neutral atmospheric hydrogen atoms can effectively remove trapped protons at energies up to 100 keV (Stuart, 1959). Most of the ENA flux in the inner magnetosphere is produced through charge exchange processes between energetic ring current ions and cold hydrogen from the exosphere. This is the dominant process by which particles are lost from the ring current (Blanc *et al.*, 1999).

ENA imaging (recording ENA fluxes as a function of the observational direction) represents a very useful technique to obtain information about the plasma ion composition and distribution in distant objects and regions in space.

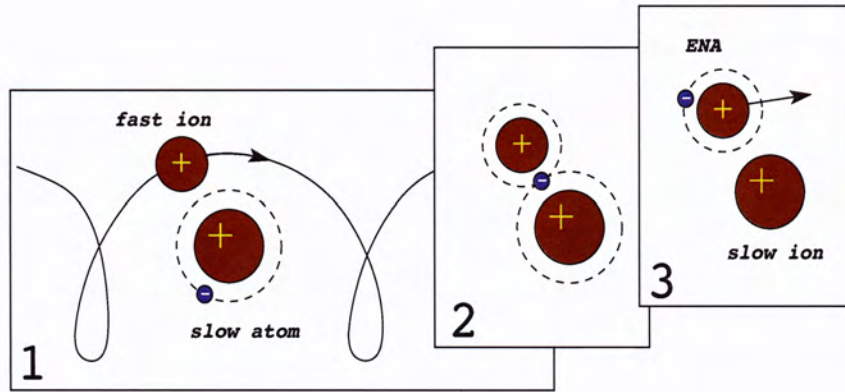


Figure 9: An energetic ion attracts an electron from a neutral atom and becomes an energetic neutral atom (ENA) during the charge exchange process. From Grigoriev, 2007.



## Chapter 8

### SUMMARY OF PAPERS

A general conclusion from our work on the low-energy (40 – 200 eV) planetary ion outflow is that ion energization and outflow occur in the sub-auroral region. The energization of the low-energy ions may take place at all altitudes. By adding the ion outflow from both hemispheres we compute a net planetary ion outflow. To avoid bad statistics we only include fluxes larger than 100 particles/(cm<sup>2</sup> s sr keV) in our computations. We estimate the low-energy ion outflow by subtracting trapped particles (assumed to be in pitch-angles between 60° and 120°) from the net ion outflow. A net ion outflow is obtained when there is a bidirectional outflow superposed on an isotropic distribution. On the other hand, an outflow embedded in an isotropic distribution gives zero ion outflow with our method.

#### **Paper 1**

In this paper we study proton and heavy ion outflow as a source for sub-keV sub-auroral/inner magnetosphere ions. We have examined two years (2001 and 2002) of the Cluster CIS data of H<sup>+</sup>, He<sup>+</sup> and O<sup>+</sup> ions in the energy range 40 – 200 keV when the Cluster spacecraft traversed the inner magnetosphere. From the database we investigated three events in more detail: 21 August 2001, 26 November 2001 and 20 February 2002. The three events were observed during different magnetic local times (MLT) and with different  $L$  values. We observed plasma outflow along magnetic field lines during quiet geomagnetic periods. The observations indicate that there is a continuous supply of energized ionospheric ions into the ring current during geomagnetic quiet conditions and independent of the MLT. The low-energy ion outflow display dispersed signatures in the energy-time spectrograms and we argue that the ultimate source of dispersed ions is upwelling terrestrial ions (e.g., Ebihara *et al.*, 2001). We have also investigated the ion composition of the outflow. The ion composition indicates that the source of the terrestrial plasma outflow covers a range of altitudes, from the low-altitude ionosphere to the plasmasphere.

#### **Paper 2**

In this paper we have made a statistical analysis of the low-energy (40 – 200 eV) ion outflow from the Earth's ionosphere into the inner magnetosphere during the most recent solar maximum. In the past, many studies have been made of the acceleration and escape of O<sup>+</sup> from the Earth's ionosphere (Shelley *et al.*, 1976; Sharp *et al.*, 1977; Mizera and Fennel, 1977; Ungstrup *et*

*al.*, 1979; Klumpar *et al.*, 1979 and Moore *et al.*, 1980). Collin *et al.* (1993) showed with an empirical model that the magnetic activity has a large influence on the outflow of low-energy O<sup>+</sup> ions. We have examined three and a half years (January 2001 – May 2004) of Cluster CIS data. From the database we have used 176 passages with sufficient coverage of the inner magnetosphere to study how the H<sup>+</sup>, He<sup>+</sup> and O<sup>+</sup> ion outflow varied with geomagnetic activity ( $K_p$ ) and magnetic local time (MLT). The result of the investigation shows that the outflow of H<sup>+</sup>, He<sup>+</sup> and O<sup>+</sup> ions increases with increasing  $K_p$  in the dawn, noon and dusk sectors, but for the midnight sector the ion outflow decreases with increasing  $K_p$ . We argue that the result may be due to two different ion sources contributing in the midnight sector. The two different sources are: 1) the nightside ionosphere and 2) a combination of the polar wind and the dayside cleft ion fountain. The two latter sources are known to be less dependent on  $K_p$ . For the dawn, noon and dusk sectors, the low-energy ion sources seem to be the ionosphere and the plasmasphere, as indicated by the composition of the ion outflow. We have also estimated the total low-energy ion outflow rates into the inner magnetosphere independently of the MLT:  $4.2 \cdot 10^{26} \text{ s}^{-1}$  for H<sup>+</sup>,  $7.1 \cdot 10^{25} \text{ s}^{-1}$  for He<sup>+</sup> and  $3.2 \cdot 10^{26} \text{ s}^{-1}$  for O<sup>+</sup>.

## Acknowledgements

### **Jag vill tacka...**

... min handledare Prof. Rickard Lundin för att han med sin breda kunskap inom rymdfysik, suveräna pedagogiska färdighet och tålamod har hjälpt mig att komma så här långt i min forskning.

... min biträdande handledare Dr. Maria Hamrin för hennes konstruktiva förslag på hur jag kan förbättra mitt författande av vetenskapliga publikationer.

... mina biträdande handledare Dr. Masatoshi Yamauchi och Dr. Hans Nilsson för att ha handlett mig under min doktorandtid på IRF i Kiruna.

... Birgitta Määttä för hennes hjälp med att få tag på vetenskapliga publikationer.

... Dr. Rick McGregor för hans hjälp med språkgranskningen av denna avhandling.

... Jonas Ekeberg, Johan Kero, Csilla Szasz och Martin Waara för alla trevliga stunder och händelser som jag fick uppleva med er under Kiruna-tiden. Tiden med er lyste upp det ibland så mörka Kiruna.

... kollegorna på IRF Umeå och Kiruna för den trevliga och vänskapliga arbetsmiljön.

... Rymdstyrelsen för finansiering av min doktorandtjänst.

... mina föräldrar, min farmor, min syster och min farbror med familj för deras ovillkorliga stöd och uppmuntran som en doktorand ganska ofta behöver.

... min hustru Binh för hennes ovärderliga stöd och kärlek.



## **Bibliography**

Banks, P. M. and Holzer, T. E.: The Polar Wind, *Journal of Geophysical Research*, Vol. 73, Issue 21, pages 6846-6854, 1968.

Bingham, R., Bryant, D. A. and Hall, D. S.: A wave model for the aurora, *Geophysical Research Letters*, Vol. 11, pages 327-330, 1984.

Blanc, M., Horwitz, J. L., Blake, J. B., Daglis, I., Lemaire, J. F., Moldwin, M. B., Orsini, S., Thorne, R. M. and Wolfe, R. A.: Source and Loss Processes in the Inner Magnetosphere, *Space Science Reviews*, Vol. 88, Issue 1/2, pages 137-206, 1999.

Bransden, B. H. and McDowell, M. R. C.: *Charge exchange and the theory of ion-atom collisions*, Oxford University Press, New York, USA, 1992.

Burch, J. L.: Low-energy electron fluxes at latitudes above the auroral zone, *Journal of Geophysical Research*, Vol. 73, pages 3585-3591, 1968.

Chappell, C. R.: The terrestrial plasma source: A new perspective in solar-terrestrial processes from Dynamics Explorer, *Reviews of Geophysics*, Vol. 26, pages 229-248, 1988.

Chen, F., F.: *Introduction to plasma physics and controlled fusion*, Volume 1: Plasma physics, Plenum Press, Second edition, New York, USA, 1984.

Cornwall, J. M.: Cyclotron Instabilities and electromagnetic emission in the ultra low frequency and very low frequency ranges, *Journal of Geophysical Research*, Vol. 70, Issue 1, pages 61-69, 1965.

Davis, L. R., Berg, O. E. and Meredith, L. H.: Direct measurements of particle fluxes in and near auroras, in *Proc. Cospar Space Sci. symposium*, North Holland Publishing Company, Amsterdam, Netherlands, 1960.

Dungey, J. W.: Interplanetary magnetic field and the auroral zones, *Physical Review Letters*, Vol. 6, pages 47-48, 1961.

Ebihara, Y., Yamauchi, M., Nilsson, H., Lundin, R. and Ejiri, M.: Wedge-like dispersion of sub-keV ions in the dayside magnetosphere: Particle simulation and Viking observation, *Journal of Geophysical Research*, Vol. 106, No. A12, pages 29571-29584, 2001.

Fel'dshteyn, Ya. I.: Some problems concerning the morphology of auroras and disturbances at high latitudes, *Geomagnetism Aeronomy*, Vol. 3, pages 183-192, 1963.

Fälthammar, C.-G.: *Space physics*, Lecture notes, Second edition, Stockholm, Sweden, 2001.

Grigoriev, A.: *The neutral particle detector on the Mars and Venus Express missions*, Doctoral thesis, ISSN 0284-1703, Swedish Institute of Space Physics, Kiruna, Sweden, 2007.

Hardy, D. A., Gussenhoven, M. S. and Holeman, E.: A statistical model of auroral electron precipitation, *Journal of Geophysical Research*, Vol. 90, pages 4229-4248, 1985.

Hoffman, J. H., Dodson, W. H., Lippincott, C. R. and Hammack, H. D.: Initial ion composition results from the Isis 2 satellite, *Journal of Geophysical Research*, Vol. 79, No. 28, pages 4246-4251, 1974.

Hones, E. W. Jr., Asbridge, J. R., Bame, S. J., Montgomery, M. D., Singer, S., Akasofu, S.-I.: Measurements of magnetotail plasma flow made with Vela 4B, *Journal of Geophysical Research*, Vol. 77, pages 5503 – 5522, 1972.

Horne, R. B. and Thorne, R. M.: On the preferred source location for the convective amplification of ion cyclotron waves, *Journal of Geophysical Research*, Vol. 98, No. A6, pages 9233-9247, 1993.

Horwitz, J. L.: Core plasma in the magnetosphere, *Reviews of geophysics*, Vol. 25, No. 3, pages 579-587, 1987.

[http://www.igpp.ucla.edu/public/THEMIS/SCI/Pubs/Nuggets/PS\\_ring\\_current/Penetration%20of%20plasma%20sheet.HTML](http://www.igpp.ucla.edu/public/THEMIS/SCI/Pubs/Nuggets/PS_ring_current/Penetration%20of%20plasma%20sheet.HTML)

<http://www-istp.gsfc.nasa.gov/istp/outreach/workshop/bobwhere.html>

Hultqvist, B., André, M., Christon, S. P., Paschmann, G. and Sibeck, D. G.: Contributions of different source and loss processes to the plasma content of the magnetosphere, *Space Science Reviews*, Vol. 88, Issue 1/2, pages 355-372, 1999.

Høymork, S. H.: *Lower hybrid cavities and other plasma phenomena in the subauroral region*, Doctoral thesis, ISBN: 91-7191-996-1, Swedish Institute of Space Physics, Kiruna, Sweden, 2001.

Kivelson, M. G. and Russel, C. T.: *Introduction to space physics*, ISBN: 0-521-45714-9, Cambridge University Press, New York, USA, 1995.

Knight, S.: Parallel electric fields, *Planetary and Space Science*, Vol. 21, Issue 5, pages 741-750, 1973.

Kozyra, J. U., Cravens, T. E., Nagy, A. F., Fonthelm, E. G. and Ong, R. S. B.: Effects of energetic heavy ions on electromagnetic ion cyclotron wave generation in the plasmopause region, *Journal of Geophysical Research*, Vol. 89, pages 2217-2233, 1984.

McIlwain, C. E.: Direct measurement of particles producing visible auroras, *Journal of Geophysical Research*, Vol. 65, pages 2727-2747, 1960.

Meng, C.-I. and Anderson, K. A.: A layer of energetic electrons (>40 keV) near the magnetopause, *Journal of Geophysical Research*, Vol. 75, Issue 10, pages 1827-1836, 1970.

Meredith, L. H., Davis, L. R., Heppner, J. P. and Berg, O. E.: *IGY Rocket Rep. Ser. 1*, National Academy of Sciences, Washington, DC, 1958.

Parks, G. K.: *Physics of space plasmas, An introduction*, ISBN: 0-8133-4130-2, Westview Press, Boulder, USA, 2004.

Paschmann, G., Haaland, S. and Treumann, R.: Auroral Plasma Physics, *Space Science Reviews*, Vol. 103, Issue 1, 2002.

Peterson, W. K., Shelley, E. G., Haerendel, G. and Paschmann, G.: Energetic ion composition in the subsolar magnetopause and boundary layer, *Journal of Geophysical Research*, Vol. 87, pages 2139-2145, 1982.

Roederer, J. G.: *Dynamics of geomagnetically trapped radiation*, Vol. 2, Springer-Verlag Berlin, Heidelberg, Germany, 1970.

Shelley, E. G., Johnson, R. G. and Sharp, R. D.: Satellite observations of an ionospheric acceleration mechanism, *Geophysical Research Letters*, Vol. 3, pages 654-656, 1976.

Sonnerup, B. U. O., Paschmann, G., Papamastorakis, I., Sckopke, N., Haerendel, G., Bame, S. J., Asbridge, J. R., Gosling, J. T. and Russell, C. T.: Evidence for magnetic field reconnection at the earth's magnetopause, *Journal of Geophysical Research*, Vol. 86, pages 10049-10067, 1981.

Stuart, G. W.: Satellite-measured radiation, *Physical Review Letters*, Vol. 2, Issue 10, pages 417-418, 1959.

Wikipedia,  
[http://upload.wikimedia.org/wikipedia/commons/9/94/Dipole\\_field.svg](http://upload.wikimedia.org/wikipedia/commons/9/94/Dipole_field.svg).

Williams, D. J.: Observations of significant magnetosheath antisolar energy flow, *Journal of Geophysical Research*, Vol. 84, pages 2105-2108, 1979.

Williams, D. J.: The Earth's ring current: causes, generation, and decay, *Space Science Reviews*, Vol. 34, pages 223-234, 1983.

Wurz, P.: Detection of energetic neutral atoms, *The outer heliosphere: beyond the planets*, pages 251 – 288, Copernicus-Gesellschaft, Katlenburg-Lindau, Germany, 2000.

## **List of acronyms**

CIS	Cluster Ion Spectrometry
CME	Corona Mass Ejection
CODIF	Composition and Distribution Function (instrument in CIS)
EMIC	Electromagnetic Ion Cyclotron
ENA	Energetic Neutral Atom
EUV	Extreme Ultra-Violet
GSM	Geocentric Solar Magnetospheric
IMF	Interplanetary Magnetic Field
MLT	Magnetic Local Time



# **PAPER I**

**Outflowing protons and heavy  
ions as a source for the sub-  
keV ring current**



## Outflowing protons and heavy ions as a source for the sub-keV ring current

T. T. Giang<sup>1</sup>, M. Hamrin<sup>2</sup>, M. Yamauchi<sup>1</sup>, R. Lundin<sup>1</sup>, H. Nilsson<sup>1</sup>, Y. Ebihara<sup>3</sup>, H. Rème<sup>4</sup>, I. Dandouras<sup>4</sup>, C. Vallat<sup>5</sup>, M. B. Bavassano-Cattaneo<sup>6</sup>, B. Klecker<sup>7</sup>, A. Korth<sup>8</sup>, L. M. Kistler<sup>9</sup>, and M. McCarthy<sup>10</sup>

<sup>1</sup>Swedish Institute of Space Physics, Kiruna, Sweden

<sup>2</sup>Department of Physics, Umeå University, Umeå, Sweden

<sup>3</sup>Institute for Advanced Research, Nagoya University, Japan

<sup>4</sup>Centre d'Etude Spatiale des Rayonnements, Toulouse, France

<sup>5</sup>VEGA contracted to Solar System Science Operations Division, ESA/ESAC, Madrid, Spain

<sup>6</sup>L'Istituto di Fisica dello Spazio Interplanetario, Roma, Italy

<sup>7</sup>Max Planck Institute for Extraterrestrial Physics, Garching, Germany

<sup>8</sup>Max-Planck-Institut für Sonnensystemforschung, Katlenburg-Lindau, Germany

<sup>9</sup>University of New Hampshire, Durham, New Hampshire, USA

<sup>10</sup>University of Washington, Seattle, USA

Received: 8 April 2008 – Revised: 14 January 2009 – Accepted: 22 January 2009 – Published: 19 February 2009

**Abstract.** Data from the Cluster CIS instrument have been used for studying proton and heavy ion ( $O^+$  and  $He^+$ ) characteristics of the sub-keV ring current. Thirteen events with dispersed heavy ions ( $O^+$  and  $He^+$ ) were identified out of two years (2001 and 2002) of Cluster data. All events took place during rather geomagnetically quiet periods. Three of those events have been investigated in detail: 21 August 2001, 26 November 2001 and 20 February 2002. These events were chosen from varying magnetic local times (MLT), and they showed different characteristics.

In this article, we discuss the potential source for sub-keV ring current ions. We show that: (1) outflows of terrestrial sub-keV ions are supplied to the ring current also during quiet geomagnetic conditions; (2) the composition of the outflow implies an origin that covers an altitude interval from the low-altitude ionosphere to the plasmasphere, and (3) terrestrial ions are moving upward along magnetic field lines, at times forming narrow collimated beams, but frequently also as broad beams. Over time, the ion beams are expected to gradually become isotropised as a result of wave-particle interaction, eventually taking the form of isotropic drifting sub-keV ion signatures. We argue that the sub-keV energy-time dispersed signatures originate from field-aligned terrestrial ion energising and outflow, which may occur at all local times and persist also during quiet times.

**Keywords.** Magnetospheric physics (Magnetosphere-ionosphere interactions; Magnetospheric configuration and dynamics; Plasma convection)

### 1 Introduction

The ring current consists of particles trapped in the geomagnetic field. The ring current varies with time and causes a slight decrease of the Earth's surface magnetic field during magnetic storms (Williams, 1983). Energetic ions drift westwards due to the gradient-curvature drift being larger than the  $E \times B$  drift ( $v = \frac{m}{2qB^2} (v_{\perp}^2 + 2v_{\parallel}^2) \mathbf{e} \times \nabla_{\perp} \mathbf{B} - E \times \mathbf{B}$ ), while the eastward  $E \times B$  drift dominates electrons and low energy ions. For intermediate energies, the drift motion is more complex, and the ions experience a competition between the gradient-curvature and  $E \times B$  drift, with the gradient-curvature drift slowing down the eastward  $E \times B$  motion. Eastward-drifting low-energy ions are predominantly of ionospheric origin; therefore, the issue of the low-energy wedge-like structures (energy-latitude dispersion structures) discussed by Yamauchi et al. (1996, 2005, 2006) and Ebihara et al. (2001) is largely a matter of the sources and losses of the ionospheric plasma.

The knowledge of heavy ionospheric ions in the ring current and plasma sheet dates back to the early 1970s. The first observations of energetic ionospheric heavy ions in the magnetosphere were made by Shelley et al. (1972). The data was



Correspondence to: T. T. Giang  
(tony.giang@irf.se)

obtained from a set of ion mass spectrometers that covered the energy range from 0.7 keV to 12 keV on board the polar-orbiting satellite 1971-089A. This satellite had a nearly circular orbit with an altitude at 800 km covering 03:00–15:00 local time (LT). They concluded that the observed precipitation of heavy ions ( $O^+$ ) is of ionospheric origin. Since then, a number of observations pertaining to the contribution of heavy ionospheric ions to the ring current have been made.

This study is concerned with the details of sub-auroral sub-keV ions. Studies of this region have been made by, e.g., GEOS-1 and Prognos-7. Geiss et al. (1978) and Balsiger et al. (1980) used data from the Ion Composition Experiment (ICE) onboard the GEOS-1 spacecraft. Regarding the thermal plasmasphere population ( $\sim 1$  eV/e), they found that it comprised of  $H^+$ ,  $O^+$ ,  $He^+$ ,  $D^+$ ,  $He^{2+}$  and  $O^{2+}$  ions, with a predominance of  $H^+$ ,  $He^+$  and  $O^+$  in order of abundance. For the low-energy ions, they found that  $H^+$  dominates over the heavy ions during magnetically quiet periods. Both Geiss et al. (1978) and Balsiger et al. (1980) concluded that the solar wind and the ionosphere are the two major sources of hot plasma in the magnetosphere. Regarding more energetic ions, Balsiger et al. (1980) and Lundin et al. (1980) found a strong depletion of  $H^+$  ions in the inner ring current as a result of charge-exchange (Tinsley, 1981), leaving the inner part of the ring current dominated by heavy ionospheric ions. However, while these heavy ions are the remains of past ionospheric ion outflow, little is known regarding sub-auroral latitudes as a region of ionospheric ion outflow. Chappell et al. (1982) made observations of the pitch-angle distribution and ion composition of thermal plasma in the inner magnetosphere using the Retarding Ion Mass Spectrometer (RIMS) instrument on board the Dynamics Explorer satellite (DE-1). The energy range of the data is up to 50 eV. They found complex characteristics of the ions, including field-aligned distributions, suggesting that the magnetosphere is fed by ions from the ionosphere and plasmasphere. Horwitz (1987) proposed an additional injection path from the dayside cleft-region into the inner magnetosphere, introducing the notion of “core plasma” for low-energy ions populating the inner magnetosphere.

Regarding ion precipitation, Sauvaud et al. (1981) observed two types of ion precipitation in the auroral and sub-auroral night-time zone (approximately 00:00–06:00 MLT) using the data from the polar orbiting satellite Aureol 1 (apogee at 2500 km and perigee at 411 km). The energy range for the measured auroral ions is from 0.4 keV to 30 keV. They concluded that the low-energy ions observed at sub-auroral latitudes are related to the eastward drift of trapped particles originating from the injection boundary during increasing AE index, i.e., when plasma sheet ions are injected into the inner magnetosphere. Using data from the F6 and F7 DMSP spacecraft, which have a sun-synchronous (08:30 MLT) circular polar orbit at 850 km altitude, Newell and Meng (1986) observed isolated and latitudinal narrow regions of ion precipitation with energies up to 1 keV in

the sub-auroral region. They concluded that cold plasma from the plasmasphere can be mixed with the warm magnetospheric plasma during substorm activities and transported from post midnight to circa 08:30 MLT.

The sub-keV ions in the inner magnetosphere region have been investigated using data from the P78-2 satellite. This satellite was in an elliptical equatorial orbit with an apogee of  $\sim 7.8 R_E$  and a perigee of  $\sim 5.3 R_E$ . The studies showed that the low-energy ion distributions are field-aligned, while the high-energy ions are peaked perpendicular to the magnetic field (Fennell et al., 1981; Kaye et al., 1981). The distributions were named ion “zipper” distributions due to a peculiar zipper-like feature observed in the ion spectrograms at the transition (in energy) from predominantly field-aligned fluxes to predominately trapped fluxes. The field-aligned ion distributions will become isotropised over time and give rise to ion energy-latitude dispersed structures, denoted as wedge-like structures by Yamauchi et al. (1996, 2005, 2006). Observations by Fennell et al. (1981) and Kaye et al. (1981) were carried out at  $L$ -values  $\sim 5.5$ – $7.7$  and during all magnetic local times. The authors concluded that the source of the high-energy ions is the plasma sheet, while the low-energy ions are of ionospheric origin.

Yamauchi et al. (1996) observed energy-latitude dispersive structures of trapped ions in the sub-keV energy range inside the ring current region. These wedge-like structures are frequently observed in the dayside sub-auroral region. Recently, statistical studies were performed on the occurrence of the wedge-like structures at different altitudes and different local times. Satellites such as Viking (mid-altitude at 5000–13 000 km), Freja (1600 km) and the Cluster satellites ( $> 4 R_E$ ) (Yamauchi et al., 1996, 2005, 2006; Ebihara et al., 2001, 2008; Yamauchi and Lundin, 2006) have been used for this purpose. All observations showed that the occurrence probability of wedge-like structures gradually decreases from morning to noon and from noon to evening, with the peak in the early morning sector.

Using a particle drift simulation, Ebihara et al. (2001) reproduced the wedge-like structures of the sub-keV ions during geomagnetic disturbed conditions by assuming that (1) the source ions are injected from the near-Earth tail to the midnight sector, (2) the source distribution function in the midnight ( $L=10$ ) is isotropic Maxwellian with a temperature of 5 keV and number density of  $0.3 \text{ cm}^{-3}$ , and (3) the ions are drifting in a co-rotational electric field, a dipole magnetic field and the Volland-Stern type convection electric field (Volland, 1973; Stern, 1975; Maynard and Chen, 1975). In their particle drift simulation, they observed three types of wedge-like structures, which were named types 1, 2 and 3, each exhibiting different characteristics. Type 1: the energy increases with invariant latitude (ILAT); Type 2: the energy increases with ILAT and then subsequently decreases with ILAT; Type 3: the energy decreases with ILAT. The successful reproduction of the dispersion patterns by Ebihara et al. (2001) indicates that the wedge-like structures could be

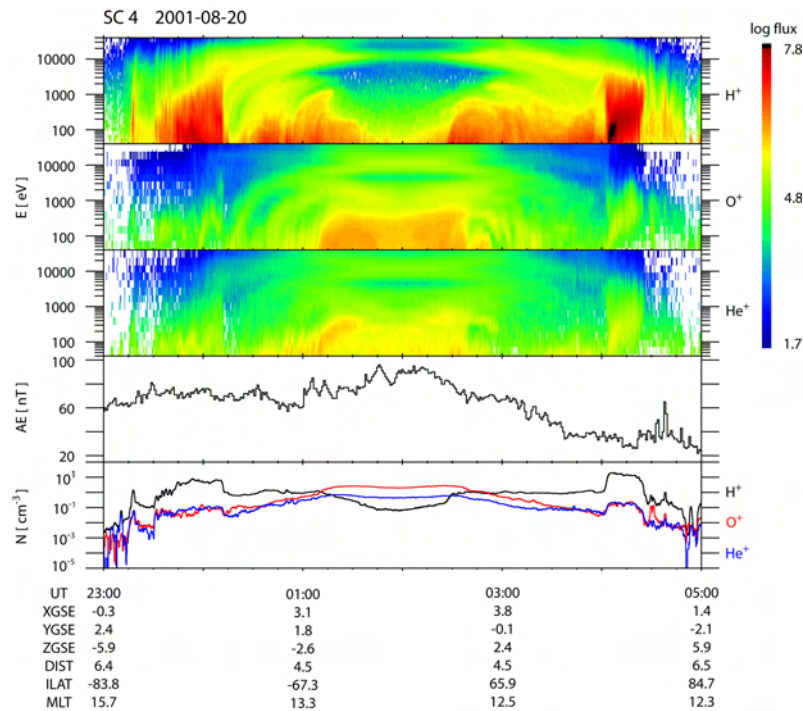


**Fig. 1.** Energy-time spectrograms over  $4\pi$  average differential fluxes in  $[(\text{cm}^2 \text{ sr keV})^{-1}]$ , AE and density plot of  $\text{H}^+$ ,  $\text{O}^+$  and  $\text{He}^+$  in the energy range of 0.04 keV to 40 keV for the entire pericentre pass of the 20–21 August 2001.

related to past substorm activities many hours before. Vallat et al. (2007) have also reproduced some of the dispersive ion structures by using numerical simulations of particle trajectories.

Yamauchi and Lundin (2006) confirmed that the wedge-like structures are related to past AE activities, and that the wedge-like trapped ions at mid-latitudes are most likely the same as the detached ions in the sub-auroral region observed by polar orbiting satellites as described above. They found that there is no relation between the wedge-like structures and  $D_{st}$  indices. They also raised questions on (1) the source location and (2) the drift velocity. The drift time from the source to the dayside statistically obtained from their backward superposed epoch analyses is much shorter (by a factor of 2–3) than in the simulation by Ebihara et al. (2001) with nearly zero lag time from substorm onset to the appearance of the wedge-like structure in the morning sector (Yamauchi and Lundin, 2006).

Yamauchi and Lundin (2006) also found that the wedge-like structures seen in the evening sector have travelled from

the morning sector by an eastward drift beyond what the model predicts. Their statistics indicate that a substantial percentage of these structures are instead formed in the morning sector during substorms. They could not identify the absolute source locations and the formation processes of the source particles ( $\text{O}^+$  and  $\text{H}^+$ ). The source problem is again discussed by Yamauchi et al. (2006) using Cluster data, confirming that some of the structures must have begun to form their energy dispersion in the morning sector. They also suggested that the  $\text{O}^+$  and  $\text{H}^+$  sources might not be located at the same magnetic local time. The source problem might also be related to the  $\text{O}^+/\text{H}^+$  ratio problem reported in Yamauchi et al. (2005).

To elucidate the source problem, i.e., from where the  $\text{O}^+$  and  $\text{H}^+$  ions originate, we studied in more detail CIS-data from three Cluster orbits (two dayside and one nightside, see Fig. 2) during relatively quiet times when the convection electric field is expected to be weaker and more stable. We investigated possible plasma source regions for the sub-keV ring current ions by analysing in more detail the pitch-angle

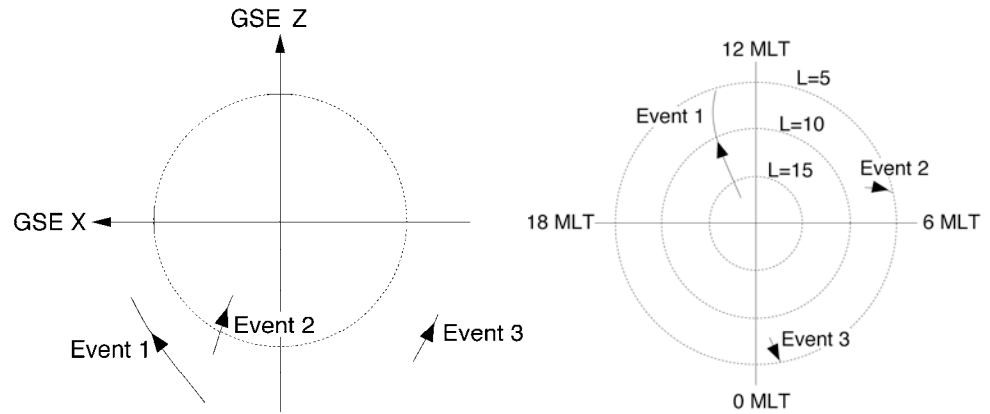


Fig. 2. Orbit projection sketches of the three traversals in X-Y GSE and MLT-L shell. For more details, see Table 1.

distributions of  $H^+$ ,  $O^+$  and  $He^+$  and comparing their density and upgoing flux ratios. In a statistical study of ring current  $H^+$  and  $O^+$  by Collin et al. (1993), some of the issues addressed here were also discussed. However, their instrument measured higher energies  $>110$  eV, and they did, for instance, not discuss time dispersion and ion outflow signatures. In this paper, we show that the upgoing ion fluxes are usually associated with energy-time dispersions signatures.

The Cluster spacecraft are placed in a polar orbit with an apogee of  $\sim 18.7 R_E$  and a perigee of  $\sim 4 R_E$ . This means that the Cluster spacecraft can reach deeper into the magnetosphere compared to the P78-2 satellite used in some earlier studies of the 1980s. In this article, the bidirectional ion outflow (upgoing ions from the Northern and Southern Hemispheres) and its relation to the evolution of sub-keV ions in the ring current are of particular interest. All three events were observed during magnetically quiet periods.

## 2 Instrumentation

We use data from the Cluster Ion Spectrometry (CIS) instrument on board the Cluster II spacecraft (SC 1, SC 3 and SC 4). CIS is an ion plasma spectrometry package capable of obtaining full three-dimensional ion distributions with good time resolution and with mass-per-charge composition determination. The CIS package consists of two different instruments, a time-of-flight ion Composition Distribution Function (CODIF), which can resolve the major magnetospheric ions, and a Hot Ion Analyser (HIA), which has no mass resolution but higher energy and angular resolution, as well as a Data Processing System (DPS), which permits on-board data processing. By using a time-of-flight technique,

CODIF can resolve  $H^+$ ,  $He^+$ ,  $He^{2+}$  and  $O^+$ . CODIF covers a  $2\pi$  field-of-view orthogonal to the spin plane with 16 detectors. This gives us the angular resolution of  $22.5^\circ$  in the spin plane. More detailed descriptions of the CIS instruments can be found in Rème et al. (2001).

## 3 Observations

We have examined two years (2001 and 2002) of Cluster CIS CODIF data of hydrogen ( $H^+$ ), oxygen ( $O^+$ ) and helium ( $He^+$ ) ions in the sub-keV energy range, 40–200 eV. In our data base, we have over 200 perigee traversals. From these traversals, we chose three events to investigate in more detail: 21 August 2001, 26 November 2001, and 20 February 2002. All three events were observed during different magnetic local times and with different L values (14.0–13.2 MLT and  $45\text{--}10 R_E$ ; 7.1–6.9 MLT and  $11\text{--}6.5 R_E$ ; 0.6–0.7 MLT and  $8\text{--}5 R_E$ ), but they all showed plasma outflow along magnetic field lines during low geomagnetic activities. This suggests an almost continuous supply of energised ionospheric ions into the ring current for all MLT and during magnetically quiet periods. Figure 2 shows the orbit projection in GSE X-Y and in MLT-L shell of our three events. From our observation, we will also be able to draw conclusions regarding the source of these upgoing ions.

The top three panels of Fig. 1 show the  $H^+$ ,  $O^+$  and  $He^+$  energy-time spectrograms for the entire pericentre pass of the 21 August event. The two bottom panels in Fig. 1 show the AE index and the number density of  $H^+$ ,  $O^+$  and  $He^+$  ions in the energy range 40–40 000 eV. From the spectrograms, one may also distinguish energy-time dispersed structures as reported by Yamauchi et al. (1996). It should be noted,

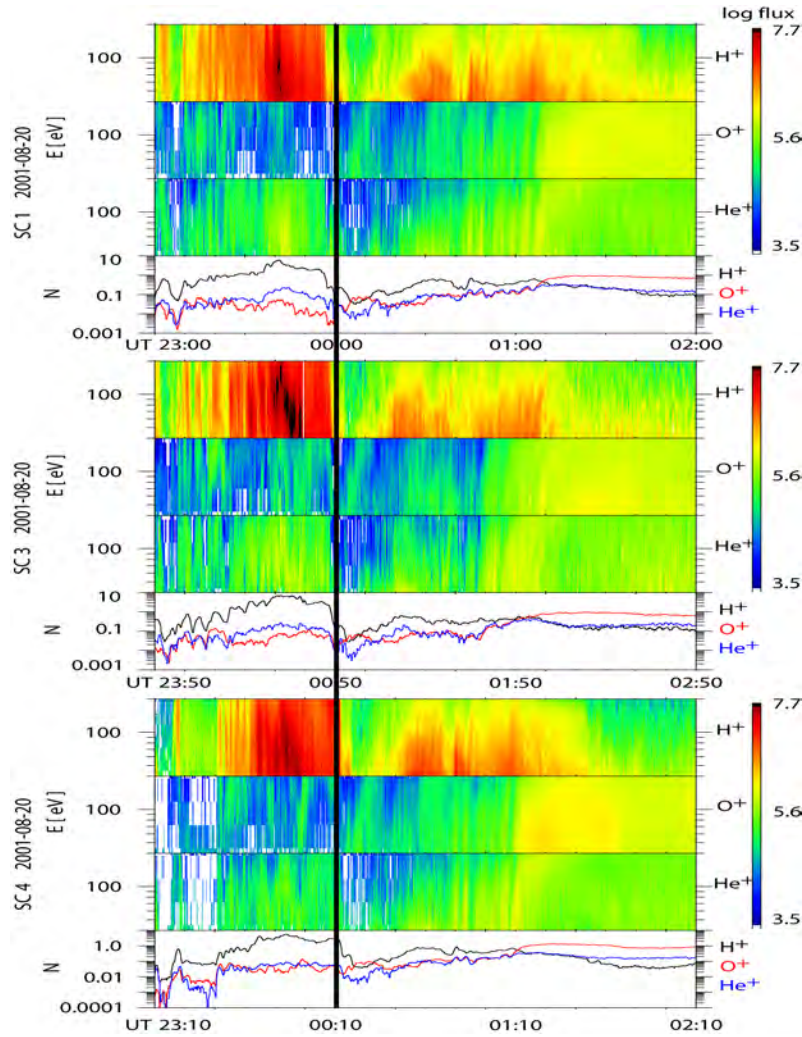


**Fig. 3.**  $H^+$ ,  $O^+$  and  $He^+$  energy-time spectrograms in  $[(cm^2 \text{ s sr keV})^{-1}]$  for 20–21 August 2001 in the energy range of 0.04 keV to 0.2 keV. The spectrograms and number density in  $[cm^{-3}]$  plots are time-shifted for the Cluster spacecraft, SC 3 and SC 4 compare to SC 1. The black line indicates the same energy-time dispersed signature for  $O^+$ .

however, that our focus is not on the energy-time dispersed signatures as such, but rather on the ion outflow signatures related with them. A strong decrease/void of energetic  $H^+$  can be seen near the pericentre, as shown in Fig. 1. This is most likely an effect of charge exchange, removing keV  $H^+$  more

effectively than  $O^+$  and  $He^+$  (e.g. Tinsley, 1981; Roelof et al., 1985). The  $H^+$  charge exchange cross-section is much higher than the  $O^+$  and  $He^+$  cross-sections. The data in Fig. 1 are from a geomagnetically quiet period, the last sub-storm injection being some 72 h ago; i.e. there is sufficient

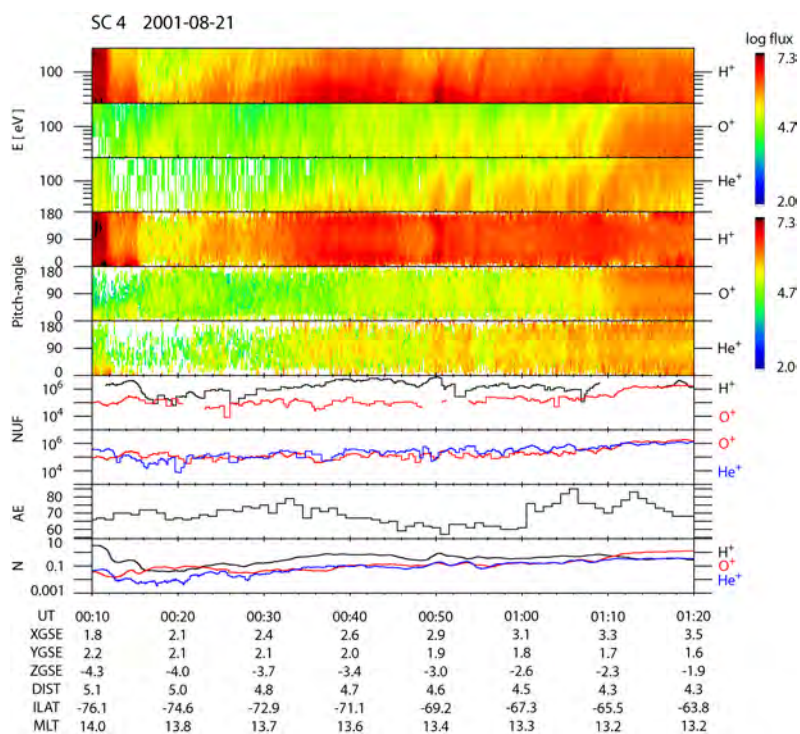


**Fig. 4.** Energy-time spectrograms, pitch-angle distributions [ $\text{cm}^2 \text{sr keV}^{-1}$ ], net upgoing fluxes (NUF) in [ $\text{cm}^{-2} \text{s}^{-1}$ ], AE in [nT] and density plot in [ $\text{cm}^{-3}$ ] in the energy range of 40 eV to 200 eV (low energy) for  $\text{H}^+$ ,  $\text{O}^+$  and  $\text{He}^+$  during the period from 00:10 UT through 01:20 UT, on 21 August 2001.

time for charge-exchange to remove a large fraction of the keV  $\text{H}^+$ . From the bottom panel of Fig. 1, we also note that the  $\text{He}^+$  content is relatively high compared to  $\text{O}^+$ , except in the inner ring current, where  $\text{O}^+$  is the most abundant ion species. This is another indication of charge exchange.

As already noted, all three events to be discussed in this article took place during relatively quiet periods, as seen from the AE indices displayed in the figures and IMF discussed. The median and mean values of the 13  $D_{st}$  indices were  $-8 \text{ nT}$  and  $-15 \text{ nT}$ , respectively, which is another indication of relatively quiet conditions. Moreover, the values of 2 out of 13 of the  $D_{st}$  indices were even positive (8 June 2001 and 21 August 2001).

### 3.1 Event 1: 21 August 2001

Figure 3 shows a zoom in the  $\text{H}^+$ ,  $\text{O}^+$  and  $\text{He}^+$  energy-time spectrograms and density of 21 August 2001. The MLT is approximately 14.0–13.2. The spectrograms and densities were

calculated in the low energy range of 0.04 keV–0.2 keV. The spectrograms and density plots are time shifted for the Cluster spacecraft 3 and 4 to be comparable with spacecraft 1. One can recognise some minor differences between the three spacecraft. Even if there are some spatial and temporal differences between the spacecraft (even after time shifting), the overall appearances of the energy-time dispersed signatures are the same for all three spacecraft. Hence, we conclude that these energy-time dispersed signatures are rather stationary in time. Since the data are very similar on all spacecraft, we chose only to investigate data from SC 4.

Figure 4 shows the energy-time spectrograms, pitch-angle distributions of the differential flux, net upgoing flux and density plots for  $\text{H}^+$ ,  $\text{O}^+$  and  $\text{He}^+$  ions during the period from 00:10 UT through 01:20 UT, on 21 August 2001. In the low energy data (0.04 keV–0.2 keV) presented in the top three panels of Fig. 4, one can recognise clear energy-time dispersed signatures for  $\text{H}^+$ ,  $\text{O}^+$  and  $\text{He}^+$  ions in two time

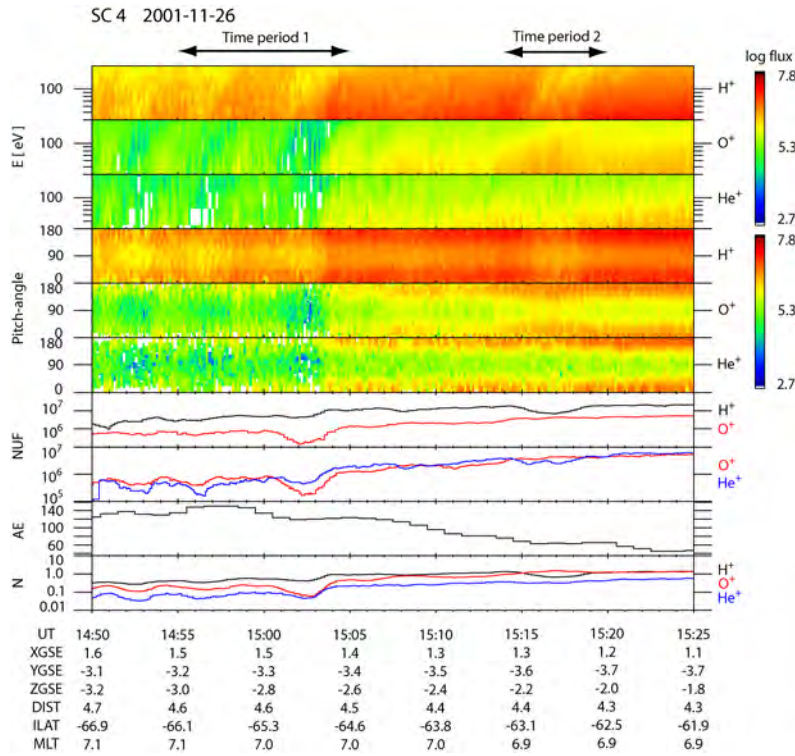


**Fig. 5.** Energy-time spectrograms, pitch-angle distributions [ $(\text{cm}^2 \text{sr keV})^{-1}$ ], net upgoing fluxes (NUF) in [ $\text{cm}^{-2} \text{s}^{-1}$ ], AE in [nT] and density plot in [ $\text{cm}^{-3}$ ] in the low energy range of 40 eV to 200 eV for  $\text{H}^+$ ,  $\text{O}^+$  and  $\text{He}^+$  during the period from 14:50 UT through 15:25 UT, on 26 November 2001.

intervals, 00:39 UT–00:50 UT and 00:52 UT–01:09 UT. The following assumptions are made in computing the net upgoing flux of planetary ions.

1. Energising of planetary ions may take place at all altitudes, from the lower ionosphere to the high-altitude ionosphere/plasmasphere.
2. Ion energising is primarily driven by waves (see, e.g. Moore et al., 1999, for a review). Transverse (to the magnetic field) energising of ions by waves leads to a diverging magnetic dipole field and, eventually, to a “conical” distribution.
3. Further energising and wave-broadening with altitude leads to further widening of the “ion conics,” such that instead of a beam-like folded conic, a wider beam with respect to pitch angle forms (see, e.g., panels 5 and 6

in Fig. 5). An ion source close to the magnetic equator (e.g., plasmasphere) leads to even broader outflow beams.

4. Because the observations are made on closed field lines (Ring Current), ion outflow, as a consequence of wave energising, is expected to reach the equatorial plane from both hemispheres.
5. The net planetary ion outflow is determined by adding the hemispherical outflow. We then subtract the flux of trapped particles ( $60^\circ$ – $120^\circ$  pitch-angle) from the outflowing particle flux ( $0^\circ$ – $60^\circ$ ;  $120^\circ$ – $180^\circ$ ). Integrating over these angles, one finds that an isotropic distribution leads to zero upgoing flux, while, as in these cases, a bidirectional outflow superposed on an isotropic distribution gives a net upgoing flux.

**Table 1.** summarises the observations of characteristics from the three events.

Date	MLT	L	$D_{st}$ index	Solar wind
21 Aug 2001	14.0–13.2	17.4–5.1	9 nT → 17 nT	IMF $B_Z \sim 0.6$ nT
26 Nov 2001	7.1–6.9	6.5–4.5	–54 nT → –50 nT	IMF $B_Z \sim 0.3$ nT
20 Feb 2002	0.6–0.7	5.9–4.6	–9 nT → –7 nT	IMF $B_Z \sim \pm 1$ nT

The number density plot in the bottom panel of Fig. 4 shows a large amount of  $\text{He}^+$  between 00:34 UT and 01:12 UT. Panel 8 displays a corresponding increase of the  $\text{He}^+$  during this time period. A large amount of  $\text{He}^+$  suggests a plasmaspheric or a high altitude ionospheric origin, where  $\text{He}^+$  may be more abundant than  $\text{O}^+$ . Panels 4–6 in Fig. 4, showing the  $\text{H}^+$ ,  $\text{O}^+$  and  $\text{He}^+$  pitch-angle distributions and the corresponding net upgoing fluxes (panel 8), are revealing in this context. We note here that the pitch-angle distributions in the high-energy range (not shown here) are either isotropic or peaked near  $90^\circ$ . Conversely, the  $\text{H}^+$  and  $\text{He}^+$  low-energy ion distributions are strongly bidirectional, mixed with an isotropic  $\text{H}^+$  component. Panels 7–8 show, therefore, that there is a net upgoing flux of low-energy planetary ions into the ring current. The co-existence of field-aligned and isotropic distributions implies two plasma populations, upgoing plasma (magnetically connected to the source) and pre-existing isotropic drifting plasma, in other words, upgoing planetary plasma mixing with pre-existing sub-keV ring current plasma. Notice also that the dispersion signature (Fig. 4) may in this case be interpreted as the low-energy part of drifting energy-time dispersed signatures as well as a signature of direct outflow of ionospheric plasma into the ring current.

This event is observed during magnetically quiet conditions. Investigating the magnetic indices, we found that  $D_{st} \approx 17$  nT (Table 1) during the event. The AE values displayed in panel 9 in Fig. 4 were rather small. IMF measured by the Advanced Composition Explorer (ACE) was weakly positive, ( $B_z \sim 0.6$  nT, Table 1).

### 3.2 Event 2: 26 November 2001

Figure 5 shows similar data as in Fig. 4, but in this case for 26 November 2001, during 14:50–15:25 UT. MLT during the time interval varied between 7.1 and 6.9. Clear energy-time dispersed signatures occurred during two periods: 14:55 UT–15:05 UT (time period 1) and 15:14 UT–15:20 UT (time period 2).

During period 1, both the  $\text{H}^+$  flux and the  $\text{O}^+$  flux increased simultaneously. However, in period 2, the intensities were anti-correlated, with the  $\text{O}^+$  intensity increasing when the  $\text{H}^+$  intensity decreased. The anti-correlated energy-time dispersions are similar for  $\text{O}^+$  and  $\text{H}^+$ , suggesting that both  $\text{O}^+$  and  $\text{H}^+$  undergo similar drift motions. To examine these correlated and anti-correlated periods in more detail, we in-

vestigated the  $\text{H}^+$ ,  $\text{O}^+$  and  $\text{He}^+$  pitch-angle distributions. In panels 4–6 of Fig. 5, the pitch-angle distributions (0.04–0.2 keV) are displayed. From 14:55 UT–15:05 UT (period 1), we again observe bidirectional plasma outflows from the ionosphere from both hemispheres, similar to the event 1, but in this case, the outflow is more persistent and occurs for all three ion species. Mapped to the ionosphere, the outflow originates from an invariant latitude range in excess of  $3^\circ$ .

Panels 7–8, showing the net outflow of  $\text{H}^+$ ,  $\text{O}^+$  and  $\text{He}^+$ , confirm that there is an increase of the  $\text{O}^+$  upgoing flux and a decrease of  $\text{H}^+$  upgoing flux during period 2.

The number density plot (bottom panel in Fig. 5) shows higher densities for  $\text{O}^+$  compared to the  $\text{He}^+$  densities, indicating that the plasma originates from the lower part of the ionosphere.

Similar to event 1, the energy-time dispersed signatures and plasma outflows took place during low geomagnetic activities. The energy-time dispersed signatures were observed more than two days after a magnetic storm with a  $D_{st}$  peak at  $-221$  nT (not shown here). AE was fairly small, as can be seen in panel 9. More than 48 h have passed since the last substorm activity of  $\text{AE} > 500$  nT. IMF was weakly positive ( $B_z \sim 0.3$  nT, Table 1). Minor high latitude auroral activity occurred around 6 h before our observation period (around 08:31 UT–08:50 UT). The high latitude activity occurred during northward IMF, suggesting minor influences on the ring current.

### 3.3 Event 3: 20 February 2002

Figure 6 shows data from 20 February 2002; the MLT varies between 0.6–0.7 during the study period. The pitch-angle distribution of  $\text{H}^+$ ,  $\text{O}^+$  and  $\text{He}^+$  are displayed in panels 3–5. The  $\text{O}^+$  and  $\text{He}^+$  distributions are bidirectional and rather similar, with fluxes peaking at  $\leq 30^\circ$  and  $\geq 150^\circ$ , while  $\text{H}^+$  displays a lack of bidirectional outflow from the hemispheres. The narrow  $\text{O}^+$  and  $\text{He}^+$  beams suggest ion outflow from low altitudes. On the other hand, the  $\text{H}^+$  distribution is essentially isotropic. The isotropic  $\text{H}^+$  distribution could in principle result from an isotropisation in the course of the  $\text{H}^+$  outflow from a low-altitude source. On the other hand, it may also imply outflow from a low-altitude source with strong heavy ion dominance, especially  $\text{O}^+$ , into a region of pre-existing isotropic  $\text{H}^+$  ions. The latter seems more likely because the  $\text{H}^+$  distribution also contains energy-time

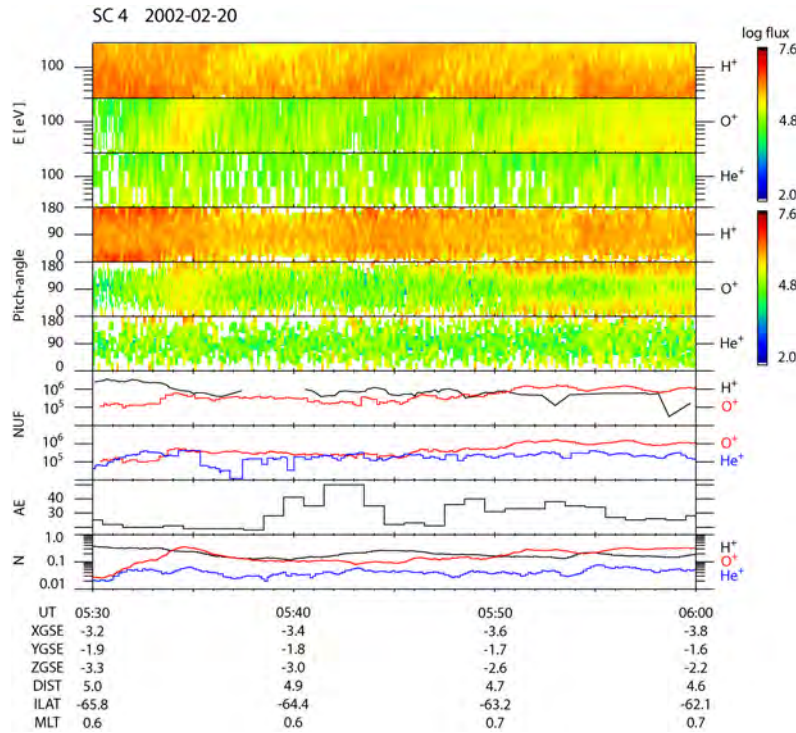


**Fig. 6.** Energy-time spectrograms, pitch-angle distributions  $[(\text{cm}^2 \text{ s sr keV})^{-1}]$ , net ongoing fluxes (NUF) in  $[\text{cm}^{-2} \text{ s}^{-1}]$ , AE in [nT] and density plot in  $[\text{cm}^{-3}]$  in the low energy range of 40 eV to 200 eV for  $\text{H}^+$ ,  $\text{O}^+$  and  $\text{He}^+$  during the period from 05:30 UT through 06:00 UT, on 20 February 2002.

dispersed signatures. In the time period 05:34 UT–05:36 UT, there is a difference between the  $\text{H}^+$  and the  $\text{O}^+$  pitch-angle distributions; the  $\text{O}^+$  flux increased while the  $\text{H}^+$  flux decreased during the same time period. A similar difference between upgoing fluxes of  $\text{H}^+$  and  $\text{O}^+$  as that observed in the time period 2 (15:14 UT–15:20 UT) in Fig. 5 is observed in panel 7 of Fig. 6, i.e., an increase of the  $\text{O}^+$  net upgoing flux when the  $\text{H}^+$  net upgoing flux shows a decrease in the time period 05:34 UT–05:36 UT. The energy-time spectrograms of the three ion species in the top three panels show several other energy-time dispersed signatures for  $\text{H}^+$ . Notice that all energy-time dispersed signatures are characterised by isotropic distributions, sometimes embedded in regions of field-aligned fluxes.

The number density plot in the bottom panel of Fig. 6 shows a higher abundance of  $\text{O}^+$  than  $\text{H}^+$  in the periods 05:34 UT–05:36 UT and 05:50 UT–06:00 UT. Our interpretation of the gradually increasing amount of  $\text{O}^+$  is that of

a source region gradually moving towards lower altitudes, where  $\text{O}^+$  becomes more abundant than  $\text{H}^+$ . Nonetheless, the overall high abundance of  $\text{O}^+$  compared to  $\text{He}^+$  suggests a low altitude ionospheric origin.

The geomagnetic activities during this event are similar to events 1 and 2, i.e., occurring during geomagnetically quiet conditions. The event was observed approximately one day after a minor magnetic storm that had ceased during the time interval discussed. Furthermore, AE (panel 9 in Fig. 6) displayed small values during the event, and the nearest substorm activity was found 30 h before this event. Thus the AE indices before and during this event are even smaller than those for the 21 August 2001, and 26 November 2001, events. The IMF changed between weakly positive and weakly negative values ( $B_z \sim \pm 1$  nT, Table 1). The timing of the energy-time dispersed signatures occurred almost at the same time as the IMF changed sign.

#### 4 Summary and discussion

In the ring current,  $H^+$ ,  $O^+$  and  $He^+$  are the dominating ions. For obvious reasons, most studies have focused on the high-energy ring current ion component and its characteristics during geomagnetic disturbed conditions. In this paper, we have focused on sub-keV (40–200 eV)  $H^+$ ,  $O^+$  and  $He^+$  ions in the ring current. The origin and characteristics of these ions have been discussed. We observed three events during relatively quiet geomagnetic periods and different magnetic local time periods, 14.0–13.2 MLT at  $L \sim 17.4$ –5.1, 7.1–6.9 MLT at  $L \sim 6.5$ –4.5 and 0.6–0.7 MLT at  $L \sim 5.9$ –4.6 (see Table 1), i.e., two events were observed on the dayside and one event on the nightside.

The three events in this paper occurred at three widely different magnetic local times and during relatively quiet geomagnetic periods. There were no major geomagnetic storms or substorms ten hours (or less) before the observations. At present, the common idea of how the energy-time dispersed signatures are created is based more or less on plasma injections from the nightside, caused by geomagnetic storms or substorms. After the nightside plasma injections, the ions then separate into two different drift directions. Depending on the energy, the ions will drift either westward or eastward (Yamauchi and Lundin, 2006). Intermediate energy ions experience a more complicated drift because of the competition between the westward gradient-curvature and the eastward  $E \times B$  drifts. The eastward ion drift increases with decreasing ion energy. The gradient-curvature drift makes the eastward drift decrease for high energy ions. Therefore, higher energy ions are slower and appear later, causing the dispersive signature.

In this article, we argue that sub-keV ions may be supplied throughout the ion drift paths and mix with the local and freshly upgoing ions. Our observations show outflow from the ionosphere intermixed with drifting energy-time dispersed plasma signatures originating from a source earlier along the ion trajectory. In event 1, the features of the  $He^+$ , panels 3 and 6 in Fig. 4, indicate such localised outflow into the ring current. We therefore argue that energy-time dispersed signatures may also be independent of the substorm activity but are formed as a consequence of the ion drifts.

The source region of the planetary ions may vary. For instance, the number density plot (bottom panel in Fig. 4) shows that the amount of  $He^+$  is higher than the amount of  $O^+$ . Since the ionosphere is stratified with respect to ion mass, this implies that the outflow in this case originates from a higher altitude, such as the plasmasphere or the polar wind. An argument for the plasmasphere as the more likely source is the transient feature of the combined  $H^+$  and  $He^+$  events, implying a more local insertion. Another, more circumstantial, alternative is that polar wind ions are transiently convected towards the dayside ring current ( $B_z > 0$ ). On the other hand, panel 5 in Figs. 5 and 6 displays an outflow dominated by  $O^+$ , implying a low-altitude ionospheric

origin below the crossover altitude where  $O^+$  begins to dominate (e.g., Moore, 1980). Altogether, our observations indicate that the ionosphere and plasmasphere may provide a steady and potentially homogeneous (with respect to MLT) contribution of sub-keV ions into the ring current, occurring also during quiet times.

Ionospheric plasma accelerated upward is expected to maintain a field-aligned pitch-angle distribution further out in the magnetosphere. Such field-aligned, beamed, pitch-angle distributions were observed in all three events in this paper (see panel 6 in Fig. 4, panels 4–6 in Fig. 5 and panels 5–6 in Fig. 6). The observed field-aligned distributions therefore represent freshly upgoing terrestrial ions into the ring current. Narrow beams imply a magnetic connection to a low-altitude source region. Conversely, broad conical shaped ion distributions suggest a close proximity to the source (e.g., in the plasmasphere), but they may also imply beam-broadening by wave-induced transverse ion energising. With time, the ion beams are expected to gradually become isotropised as a result of wave-particle interaction, eventually taking the form of isotropic drifting sub-keV ion signatures. We therefore hypothesise that the energy-time dispersed signatures originate from upgoing ion distributions that have become isotropised. The isotropic component may subsequently evolve into energy-time dispersed signatures as a result of the combined gradient-curvature and  $E \times B$  drift along the drift paths.

Eventually, the sub-keV ring current ions are subject to loss processes, such as charge exchange and ion precipitation back into the atmosphere. The fact that charge exchange processes are involved is evidenced by, e.g., Fig. 1, showing a strong decrease of sub-keV  $H^+$  fluxes in the innermost part of the orbit. For low energies ( $< 1$  keV),  $He^+$  has a much smaller charge-exchange cross section than  $O^+$  by a factor of 10 (Tinsley, 1981).

#### 5 Conclusion

We have studied the outflow of ionospheric sub-keV ions,  $H^+$ ,  $He^+$  and  $O^+$ , as an additional source for the ring current population. Three events observed during different magnetic local times and with different characteristics have been investigated and discussed. Combining ion data from three Cluster spacecraft indicates that the energy-time dispersed signatures are foremost a spatial phenomenon. From our investigation, we conclude that: (1) sub-keV ions of terrestrial origin are supplied into the ring current also during quiet geomagnetic conditions; (2) the composition of the outflow implies an origin that covers an altitude interval from the low-altitude ionosphere to the plasmasphere, and (3) terrestrial ions are moving upward along magnetic field lines, at times forming narrow collimated beams, but frequently also as broad conical shaped distributions. With time, the ion beams/conics are expected to gradually become isotropised

as a result of wave-particle interaction, eventually taking the form of isotropic drifting sub-keV ion signatures. We therefore argue that the sub-keV energy-time dispersed signatures originate from field-aligned terrestrial ion energising and outflow that may occur at all local times and also persist during quiet times.

**Acknowledgements.** The Cluster project was carried out by ESA, and the Cluster II CIS instrument was supported by ESA and built by many institutions: CESR Toulouse as PI institute, IRF Kiruna, MPE Garching, IFSI Roma, MPAE (now MPS) Lindau, U Bern, U Washington, UNH, LPARL and UCB/SSL. The AE and  $D_{st}$  indices are provided by Data Analysis Center for Geomagnetism and Space Magnetism, Kyoto University. The ACE data are provided by NOAA ACE team. The work of TTG was supported by the Swedish National Space Board.

Topical Editor I. A. Daglis thanks J. Horwitz for his help in evaluating this paper.

## References

- Balsiger, H., Eberhardt, P., Geiss, J., and Young, D. T.: Magnetic storm injection of 0.9- to 16-keV/e solar and terrestrial ions into the high-altitude magnetosphere, *J. Geophys. Res.*, 85(A4), 1645–1662, 1980.
- Chappell, C. R., Green, J. L., Johnson, J. F. E., and Waite Jr., J. H.: Pitch angle variations in magnetospheric thermal plasma – Initial observations from Dynamics Explorer-1, *Geophys. Res. Lett.*, 9(9), 933–936, 1982.
- Collin, H. L., Quinn, J. M., and Cladis, J. B.: An empirical static model of low energy ring current ions, *Geophys. Res. Lett.*, 20(2), 141–144, 1993.
- Ebihara, Y., Yamauchi, M., Nilsson, H., Lundin, R., and Ejiri, M.: Wedge-like dispersion of sub-keV ions in the dayside magnetosphere: Particle simulation and Viking observation, *J. Geophys. Res.*, 106(A12), 29571–29584, 2001.
- Ebihara, Y., Kistler, L. M., and Eliasson, L.: Imaging cold ions in the plasma sheet from the Equator-S satellite, *Geophys. Res. Lett.*, 35, L15103, doi:10.1029/2008GL034357, 2008.
- Fennell, J. F., Croley Jr., D. R., and Kaye, S. M.: Low-energy ion pitch angle distributions in the outer magnetosphere: Ion zipper distributions, *J. Geophys. Res.*, 86(A5), 3375–3382, 1981.
- Geiss, J., Balsiger, H., Eberhardt, P., Walker, H. P., Weber, L., and Young, D. T.: Dynamics of magnetospheric ion composition as observed by the GEOS mass spectrometer, *Space Sci. Rev.*, 22, 537–566, 1978.
- Horwitz, J. L.: Core plasma in the magnetosphere, *Rev. Geophys.*, 25(3), 579–587, 1987.
- Kaye, S. M., Shelley, E. G., Sharp, R. D., and Johnson, R. G.: Ion composition of zipper events, *J. Geophys. Res.*, 86(A5), 3383–3388, 1981.
- Lundin, R., Lyons, L. R., and Pissarenko, N.: Observations of the ring current composition at  $L < 4$ , *Geophys. Res. Lett.*, 7(6), 425–428, 1980.
- Maynard, N. C. and Chen, A. J.: Isolated cold plasma regions: Observations and their relation to possible production mechanisms, *J. Geophys. Res.*, 80, 1009–1013, 1975.
- Moore, T. E.: Modulation of terrestrial ion escape flux composition (by low-altitude acceleration and charge exchange chemistry), *J. Geophys. Res.*, 85(A5), 2011–2116, 1980.
- Moore, T. E., Lundin, R., Alcayde, D., Andre, M., Ganguli, S. B., Temerin, M., and Yau, A.: Source processes in the high-latitude ionosphere, Ch #2, in: *Magnetospheric Plasma Sources and Losses*, *Space Sci. Rev.*, 88, 7–84, 1999.
- Newell, P. T. and Meng, C.-L.: Substorm introduction of  $\leq 1$ -keV magnetospheric ions into the inner plasmasphere, *J. Geophys. Res.*, 91(A10), 11133–11145, 1986.
- Rème, H., Aoustin, C., Bosqued, J. M., et al.: First multispacecraft ion measurements in and near the Earth's magnetosphere with the identical Cluster ion spectrometry (CIS) experiment, *Ann. Geophys.*, 19, 1303–1354, 2001, <http://www.ann-geophys.net/19/1303/2001/>.
- Roelof, E. C., Mitchell, D. G., and Williams, D. J.: Energetic neutral atoms ( $E \sim 50$  keV) from the ring current: IMP 7/8 and SSE 1, *J. Geophys. Res.*, 90(A11), 10991–11008, 1985.
- Sauvaud, J. A., Crasnier, J., Mouala, K., Kovrazhkin, R. A., and Jorjio, N. V.: Morning sector ion precipitation following substorm injections, *J. Geophys. Res.*, 86(A5), 3430–3438, 1981.
- Shelley, E. G., Johnson, R. G., and Sharp, R. D.: Satellite observations of energetic heavy ions during a geomagnetic storm, *J. Geophys. Res.*, 77(31), 6104–6110, 1972.
- Stern, D. P.: The motion of a proton in the equatorial magnetosphere, *J. Geophys. Res.*, 80, 595–599, 1975.
- Tinsley, B. A.: Neutral atom precipitation – a review, *J. Atmos. Terr. Phys.*, 43(5/6), 617–632, 1981.
- Vallat, C., Ganushkina, N., Dandouras, I., Escoubet, C. P., Taylor, M. G. T., Laakso, H., Masson, A., Sauvaud, J.-A., Rème, H., and Daly, P.: Ion multi-nose structures observed by Cluster in the inner Magnetosphere, *Ann. Geophys.*, 25, 171–190, 2007, <http://www.ann-geophys.net/25/171/2007/>.
- Volland, H.: A semiempirical model of large-scale magnetospheric electric fields, *J. Geophys. Res.*, 78, 171–180, 1973.
- Williams, D. J.: The Earth's ring current: causes, generation, and decay, *Space Sci. Rev.*, 34, 223–234, 1983.
- Yamauchi, M., Lundin, R., Eliasson, L., and Norberg, O.: Mesoscale structures of radiation belt/ring current detected by low-energy ions, *Adv. Space Res.*, 17(2), 171–174, 1996.
- Yamauchi, M., Lundin, R., Eliasson, L., Winningham, D., Rème, H., Vallat, C., Dandouras, I., et al.: Structures of sub-keV ions inside the ring current region, *The Inner Magnetosphere: Physics and Modeling*, *Geophysical Monograph Series 155*, 41–46, 2005.
- Yamauchi, M. and Lundin, R.: Sub-keV ring current ions as the tracer of substorm injection, *Ann. Geophys.*, 24, 355–366, 2006, <http://www.ann-geophys.net/24/355/2006/>.
- Yamauchi, M., Brandt, P. C., Ebihara, Y., Dandouras, I., Nilsson, H., Lundin, R., Rème, H., Vallat, C., Lindqvist, P.-A., Balogh, A., and Daly, P. W.: Source location of the wedge-like dispersed ring current in the morning sector during a substorm, *J. Geophys. Res.*, 111, A11S09, doi:10.1029/2006JA011621, 2006.



# **PAPER II**

**Low-energy ion outflow into the  
Earth's inner magnetosphere**



# Low-energy ion outflow into the Earth's inner magnetosphere

T. T. Giang<sup>1</sup>, M. Hamrin<sup>2</sup>, R. Lundin<sup>1</sup>, H. Rème<sup>3</sup> and I. Dandouras<sup>3</sup>

<sup>1</sup>Swedish Institute of Space Physics, Umeå, Sweden

<sup>2</sup>Department of Physics, Umeå University, Umeå, Sweden

<sup>3</sup>Centre d'Etude Spatiale des Rayonnements, Toulouse, France

Submitted for publication in *Annales Geophysicae*, June 2009.

## Abstract

Data from 176 Cluster traversals of the inner magnetosphere from January 2001 to May 2004 have been used to investigate the outflow of low-energy (40 – 200 eV) H<sup>+</sup>, He<sup>+</sup> and O<sup>+</sup> ions. The variation of the outflow with geomagnetic activity ( $K_p$  index) and magnetic local time (MLT) has been studied. Our investigation showed that the ion outflow increases with  $K_p$  in the dawn, noon and dusk sectors. The ion outflow in the midnight sector, however, behaves significantly different. In that sector the ion outflow decreases with increasing  $K_p$ . We argue that the observational results in the midnight sector may be due to the fact that the ions originate from two different sources, the midnight ionosphere and the polar wind/dayside cleft ion fountain, the latter two less dependent on global magnetic disturbances ( $K_p$ ). The ion composition of the outflow in the other three MLT sectors (dawn, noon and dusk), suggests that the outflow originates from the low as well as high altitude ionosphere/plasmasphere. The estimated total outflow rate of low-energy ions into the inner magnetosphere ( $L \sim 4.5 - 8.5$ ) is  $4.2 \cdot 10^{26} \text{ s}^{-1}$  for H<sup>+</sup>,  $7.1 \cdot 10^{25} \text{ s}^{-1}$  for He<sup>+</sup> and  $3.2 \cdot 10^{26} \text{ s}^{-1}$  for O<sup>+</sup>.

## Introduction

The ionosphere is a source for hot plasma to the magnetosphere due to the outflow of energized ionospheric plasma (ion conics and beams). The ion conics and beams are the results of parallel and transverse acceleration processes in the high altitude auroral ionosphere (Shelley et al., 1976; Sharp et al., 1977; Mizera and Fennel, 1977; Ungstrup et al., 1979; Klumpar et al., 1979). Moore et al. (1980) found that acceleration processes are required for the O<sup>+</sup> ions to be able to escape from the ionosphere, and they also showed

that the composition of the ionospheric escape flux could be modulated by the interaction between the ionospheric charge exchange chemistry and the low altitude acceleration processes. Beside the acceleration processes, there may be other factors that influence the magnitude and the composition of the upflowing ionospheric ions. By using an empirical model, Collin et al. (1993) showed that the magnetic activity has a large influence on the low-energy O<sup>+</sup> outflow. The consequence is a very high outflow during high magnetic activities and a low outflow otherwise.

Large-scale plasma density depletion regions in the ionosphere, sometimes denoted ionospheric large-scale troughs, is another consequence of ionospheric ion outflow. Ionospheric troughs were first identified as large-scale regions with low electron densities in the ionosphere (e.g. Muldrew et al, 1965, Liszka, 1967). Later, troughs were also identified from *in situ* data from satellites. Analysis of data from the Explorer 32 satellite probing the mid altitude trough region ( $L = 5.0 - 10.5$ ) by Brinton et al. (1971) showed variations of the ion composition at altitudes 600 km to 2500 km. They found that the densities of H<sup>+</sup> and He<sup>+</sup> ions decrease with increasing altitude along closed field lines. Brinton and et al (1971) demonstrated that the observed large-scale density cavity distributions could only be explained by upflowing H<sup>+</sup> and He<sup>+</sup> ions.

Numerous spacecraft measurements, e.g. the University of Iowa Hawkeye satellite and the Freja satellite, observed large-scale regions with low plasma densities, denoted auroral density cavities. Calvert (1981) used data from the former satellite and showed that the auroral density cavities are associated with the acceleration of auroral electrons. Lundin et al. (1994) used data from the Freja satellite and concluded that strong energization implies low densities inside the auroral large-scale plasma density cavity.

To identify the source regions of terrestrial ions in more detail, ion composition instruments became an important part of a scientific satellite payload. This led to new findings about source and loss processes in the Earth's magnetosphere (e.g. Hultqvist et al., 1999). For instance, the ion composition data from GEOS 1 showed that the plasmasphere consists predominantly of H<sup>+</sup>, He<sup>+</sup> and O<sup>+</sup> in the sub-auroral region. Using data from the GEOS 1 satellite, Geiss et al. (1978) and Balsiger et al. (1980) observed ions in the energy range up to 16 keV. They concluded that the hot plasma in the magnetosphere, to a variable extent, is of both solar and ionospheric origin. Regarding more energetic ions, Balsiger et al. (1980) and Lundin et al. (1980) concluded that the inner part of the ring current is populated by heavy ions of ionospheric origin. The absence of H<sup>+</sup> in the inner part of the ring current is a result of a strong depletion of H<sup>+</sup> due to the charge-exchange process (Tinsley, 1981). In another ion composition study of the low-latitude region, Chappell et al. (1982) used data from the Dynamics Explorer satellite (DE-1) and they found field-aligned distributions of ions in

the energy range up to 50 eV. They suggested that the ions in the inner magnetosphere are supplied directly from the ionosphere and plasmasphere. Using data from the P78-2 satellite at L-values  $\sim 5.5 - 7.7$ , Fennell et al. (1981) and Kaye et al. (1981) showed that the distributions of high-energy ion are predominantly perpendicular to the magnetic field, while the distributions of low-energy ions are mostly field-aligned. They concluded that the high-energy ions originate from the plasma sheet and that the low-energy ions from the ionosphere. Using data from the Cluster spacecraft, Giang et al. (2009) observed a direct outflow of low-energy  $H^+$ ,  $He^+$  and  $O^+$  ions into the ring current. The ion sources of these outflows are the ionosphere and the plasmasphere.

In this paper we investigate the variation of the low-energy ion outflow with geomagnetic activities ( $K_p$  index) and magnetic local times (MLT).

## Instrumentation

The four Cluster II spacecraft were launched in 2000 and have an elliptical polar orbit. Each spacecraft carry 11 identical instruments onboard. The Cluster Ion Spectrometry (CIS) instrument is one of these instruments. The CIS instrument is able to measure the ion distributions in three dimensions. It can determine the mass and charge of the ions with good time resolution. CIS consist of two separate instruments: the Composition and Distribution Function (CODIF) and the Hot Ion Analyser (HIA). The CODIF instrument is a time-of-flight instrument that can resolve magnetospheric ions ( $H^+$ ,  $He^+$ ,  $He^{2+}$  and  $O^+$ ), while the HIA instrument cannot since it has no mass resolution. More detailed descriptions of the CIS instruments can be found in Rème et al. (2001). CIS CODIF data from Cluster spacecraft 4 have been used for this study.

## Observation

Out of three and a half years (January 2001 – May 2004) of Cluster CIS CODIF data from spacecraft 4, we have selected 176 passages of the inner magnetosphere to study the low-energy (40 – 200 eV) outflow of  $H^+$ ,  $He^+$  and  $O^+$  ions. The investigated regions correspond to latitudes near the equator, at altitudes from  $3.9 R_E$  to  $6.7 R_E$ . We have investigated the variation of the low-energy ion outflow with geomagnetic activity ( $K_p$ ) and magnetic local time (MLT).

The data are divided into bins according to the four MLT sectors: dawn (03:00 – 09:00 MLT), noon (09:00 – 15:00 MLT), dusk (15:00 – 21:00

MLT) and midnight (21:00 – 03:00 MLT). Moreover, the data have been binned into three  $K_p$  groups according to  $K_p \leq 2$ -,  $2 \leq K_p \leq 4$ - and  $K_p \geq 4$ .

To be able to compute the low-energy ion outflow, we assume that the ion energization and outflow occurs on closed magnetic field lines. The energization of cold planetary ions may take place at all altitudes, from the lower ionosphere to the high-altitude ionosphere/plasmasphere. Investigating the ion composition, we may determine the source of the ion outflow. The observations are made in the inner magnetosphere, and the ion outflow, possibly caused by wave energization, is expected to reach the equatorial plane from both hemispheres.

The net planetary ion outflow is computed by adding the ion outflow from both hemispheres. However, to avoid problems with poor statistics, we only consider fluxes larger than 100 part/(cm<sup>2</sup> s sr keV). We then subtract what we infer as trapped particles (60° - 120° pitch-angle) from the outflow above (0° - 60°; 120° - 180°). Note that an isotropic distribution leads to zero outflow, while, as in our cases, a bidirectional outflow superposed on an isotropic distribution, results in a net outflow.

Figures 1 – 4 show the average and median outflows in the low-energy range (40 – 200 eV) for H<sup>+</sup>, He<sup>+</sup> and O<sup>+</sup> ions during different geomagnetic activities. Each figure shows the result from a separate MLT sector, dawn (03 – 09 MLT), noon (09 – 15 MLT), dusk (15 – 21 MLT) and midnight (21 – 03 MLT). The broad and the narrow bars in the figures represent the average and median outflow of the ions, respectively. The 25% and 75% percentiles of the median are indicated. The statistics in the plots are based on the number of Cluster passages in the inner magnetosphere in each  $K_p$  and MLT bin as presented in Table 1.

Figures 1 – 3 show that the outflow of H<sup>+</sup> and O<sup>+</sup> ions increases with increasing geomagnetic activities ( $K_p$ ) in the dawn, noon, and dusk sectors. The average and median values of the outflow for each one of the three ion species indicate the same trend. Note, that the average O<sup>+</sup> outflow is much larger than the median outflow in the interval  $K_p \geq 4$  in the dusk sector (see Fig. 3). This is caused by one Cluster passage associated with very high flows, and which increases the average as compared to the median in this case. As expected, the He<sup>+</sup> outflow also increases with increasing  $K_p$  in the noon and the dusk sectors. In the dawn sector (see Fig. 1), the outflow of He<sup>+</sup> ions display a weak increase with  $K_p$ . Scatter plots (not shown here) also show increasing ion outflow with increasing geomagnetic activities.

The ion outflow in the midnight sector, on the other hand, behaves differently. As shown in Fig 4, in this sector the outflow of H<sup>+</sup>, He<sup>+</sup> and O<sup>+</sup> ions decrease with increasing geomagnetic activities. This result is opposite to what one would intuitively expect: increasing ion outflow with increasing geomagnetic activities.

Table 2 shows the average flux estimated for the low-energy H<sup>+</sup>, He<sup>+</sup> and O<sup>+</sup> ions within different L-ranges. To determine how sensitive the average flux is with L-value range, we have decreased the L-value range by removing outliers in  $L$  from each group. The result from Table 2 shows that the average ion flux increases, but not much, for smaller ranges of  $L$ . If anything, it shows the presence of higher ion fluxes for low L-values compared to high L-values. Table 3 and 4 show the estimated ion flux in the four MLT sectors. The values in Table 3 and 4 are based on the data from the group 1 in Table 2. The estimated average outflow rate [s<sup>-1</sup>] of low-energy ions, independently of L-value, is presented in Table 4. Note that the He<sup>+</sup> ion outflow rate is quite high, suggesting that the plasmasphere is an important source as well.

## Summary and Discussion

Ionospheric ion outflow in the inner magnetosphere are known since the beginning of the 1970 when the first mass-analyzing satellite instruments were able to identify energetic O<sup>+</sup> ions (e.g. Shelley et al., 1972). Previous studies have mostly focused on the energetic ionospheric ion outflow at high latitudes (e.g. Hoffman et al., 1974). In this paper, we have investigated the low-energy outflow at low latitudes. Three and a half years of low-energy ion outflow data measured by the CIS CODIF instrument onboard the Cluster spacecraft 4 have been analyzed. We have studied 176 Cluster passages of the inner magnetosphere in more detail. We have analyzed the variation of the low-energy ion outflow with geomagnetic activity ( $K_p$ ) and magnetic local times (MLT).

We find that the low-energy outflow of H<sup>+</sup>, He<sup>+</sup> and O<sup>+</sup> ions increase with increasing geomagnetic activity in the dawn (03 – 09 MLT), noon (09 – 15 MLT) and dusk (15 – 21 MLT) sectors. This is in good agreement with previous investigations of the high-latitude energetic ion outflow (e.g. Yau et al., 1988). A noticeable result in the dawn, noon and dusk sectors are that the O<sup>+</sup> ion outflow dominates (larger outflow) over the He<sup>+</sup> ion outflow. This indicates that the low-energy ion outflow in these sectors originates from the lower ionosphere where O<sup>+</sup> dominates over He<sup>+</sup>.

H<sup>+</sup> and O<sup>+</sup> ions dominate the outflow in the midnight sector, similar to the other three MLT sectors, hence indicating a low-altitude/mid-altitude ionospheric source region. As shown in Fig 4, the midnight sector, however, appears to be characterized by a weakly decreasing outflow of H<sup>+</sup>, He<sup>+</sup> and O<sup>+</sup> ions with increasing geomagnetic activities. This is essentially opposite to the results obtained for the other three MLT sectors and therefore requires further analysis. In this article we have focused on low-energy ions (40 – 200 eV). One might suspect that the unexpected results from the midnight

sector may be due to the energy range used. Hence we have also analyzed the energetic part (1 – 20 keV) of the ion outflow in the midnight sector. For the high-energy ion outflow, we find that the result is quite similar to the low-energy outflow. However, the high-energy component shows a more constant ion outflow versus  $K_p$ . Hence we believe that the unexpected behaviour in the midnight sector is not due to the choice of energy range. The midnight sector is therefore the only MLT sector that shows a decrease of the low-energy ion outflow with increasing geomagnetic activities.

In Fig. 4 we also see that the  $H^+$ ,  $He^+$  and  $O^+$  ion outflow are higher in the midnight sector during quiet geomagnetic activities ( $K_p \leq 2$ -) than in the dawn, noon, and dusk sectors. This may be due to different sources for the ion outflow in the midnight sector as compared to the other sectors. We believe that the dawn, noon and dusk outflow originate directly from the lower ionosphere to the high-altitude ionosphere/plasmasphere. This can be concluded from the  $O^+$  domination in the outflow. The source regions for the outflow in the midnight sector, on the other hand, may be a combination of direct ion upwelling from the nightside ionosphere/plasmasphere and ions convecting towards the nightside from the polar ionosphere and the dayside cleft ion fountain (e.g. Horwitz, 1987). The lower ionosphere and the high-altitude ionosphere/plasmasphere may hence contribute to the ion outflow during all geomagnetic conditions and all MLT sectors, while an additional source, the polar ionosphere and the dayside cleft ion fountain, also contributes, and may even dominate for the midnight sector, especially for small  $K_p$ .

The polar region and the dayside cleft ion fountain may be rather active also during quiet geomagnetic conditions (Meng, 1981; Murphree et al., 1982; Frank et al., 1982). Low-energy ions (mainly  $O^+$  ions) from the polar region and the dayside cleft ion fountain dominate the outflow during low geomagnetic activities. These ions may reach the low-latitude region especially in the midnight sector by convection. This may explain the result in Fig. 4 where we see significantly high fluxes for  $K_p \leq 2$ - in the midnight sector and a somewhat decreasing trend in the ion outflow with increasing geomagnetic activities.

Table 4 shows the ion outflow rate in each of the four MLT sectors. The outflow rate of all three ion species is quite high, and one may speculate why we observe such high fluxes. Firstly, the method used to compute the ion outflow takes into account all ions with pitch-angles between  $0^\circ - 60^\circ$  and  $120^\circ - 180^\circ$ . This is based on the fact that upgoing ions form very broad beams, i.e. we assume that the ions are energized in a wide altitude range. Secondly, field-aligned low-energy ions move very slowly (half bounce period about 11 min. for  $H^+$ , 22 min. for  $He^+$  and 43 min. for  $O^+$  with energy 100 eV and at  $L = 4.5$ ), thus staying for a long time on closed field lines, the main loss process most likely being charge-exchange (CE) with neutral gas

(atmosphere). This will lead to an accumulation of low-energy ions in the inner magnetosphere, characterized by a balance between source and loss (e.g. CE). As previously mentioned, the relatively high outflow of He<sup>+</sup> ions indicates ion energizing at high-altitudes, i.e. the plasmasphere is a potential source for low-energy ions in the inner magnetosphere.

## Conclusion

We have used the CIS CODIF data from 176 Cluster traversals of the inner magnetosphere to investigate how the low-energy (40 – 200 eV) H<sup>+</sup>, He<sup>+</sup>, and O<sup>+</sup> ion outflow vary with geomagnetic activity ( $K_p$  index) and magnetic local time (MLT). Our results show that the outflow of H<sup>+</sup>, He<sup>+</sup> and O<sup>+</sup> ions increase with increasing  $K_p$  in the dawn, noon and dusk sectors. However, the ion outflow instead decreases with increasing  $K_p$  in the midnight sector. This unexpected result may be due to the fact that two different ion sources contribute in the midnight sector, the nightside ionosphere, and a combination of the polar wind and the dayside cleft ion fountain. The two latter sources are known to be less dependent on the global magnetic disturbance level ( $K_p$ ). The upwelling low-energy ions in the other three sectors (dawn, noon and dusk) seems to originate from both the ionosphere and the plasmasphere, as indicated by the composition of the ion outflow.

The estimated total low-energy ion outflow rates into the inner magnetosphere ( $L \sim 4.5 - 8.5$ ), independently of MLT are:  $4.2 \cdot 10^{26} \text{ s}^{-1}$  for the H<sup>+</sup>,  $7.1 \cdot 10^{25} \text{ s}^{-1}$  for the He<sup>+</sup> and  $3.2 \cdot 10^{26} \text{ s}^{-1}$  for the O<sup>+</sup>.

## Acknowledgements

The Cluster project was carried out by ESA, and the Cluster II CIS instrument was supported by ESA and built by many institutions: CESR Toulouse as PI institute, IRF Kiruna, MPE Garching, IFSI Roma, MPAE (now MPS) Lindau, U Bern, U Washington, UNH, LPARL and UCB/SSL. The  $K_p$  index is provided by Data Analysis Center for Geomagnetism and Space Magnetism, Kyoto University. T. T. Giang thanks Pär-Ola Nilsson and Fredrik Rutqvist for the assistance with the software and data managements.

## Reference

Balsiger, H., Eberhardt, P., Geiss, J. and Young, D. T.: Magnetic storm injection of 0.9- to 16-keV/e solar and terrestrial ions into the high-altitude magnetosphere, *Journal of Geophysical Research*, Vol. 85, No. A4, pages 1645-1662, 1980.

Brinton, H. C., Grebowsky, J. M. and Mayr, H. G.: Altitude variation of ion composition in the midlatitude trough region: Evidence for upward plasma flow, *Journal of Geophysical Research*, Vol. 76, No. 16, pages 3738-3745, 1971.

Calvert, W.: The auroral plasma cavity, *Geophysical Research Letter*, Vol. 8, No. 8, pages 919-921, 1981.

Chappell, C. R., Green, J. L., Johnson, J. F. E. and Waite, Jr., J. H.: Pitch angle variations in magnetospheric thermal plasma – Initial observations from Dynamics Explorer-1, *Geophysical Research Letters*, Vol. 9, No. 9, pages 933-936, 1982.

Collin, H. L., Quinn, J. M. and Cladis, J. B.: An empirical static model of low energy ring current ions, *Geophysical Research Letter*, Vol. 20, No. 2, pages 141-144, 1993.

Fennell, J. F., Croley Jr, D. R. and Kaye, S. M.: Low-energy ion pitch angle distributions in the outer magnetosphere: Ion zipper distributions, *Journal of Geophysical Research*, Vol. 86, No. A5, pages 3375-3382, 1981.

Frank, L. A., Craven, J. D., Burch, J. L. and Winningham J. D.: Polar views of the Earth's aurora with Dynamics Explorer, *Geophysical Research Letters*, Vol. 9, No. 9, pages 1001-1004, 1982.

Geiss, J., Balsiger, H., Eberhardt, P., Walker, H. P., Weber, L. and Young, D. T.: Dynamics of magnetospheric ion composition as observed by the GEOS mass spectrometer, *Space Science Reviews*, 22, pages 537-566, 1978.

Giang, T. T., Hamrin, M., Yamauchi, M., Lundin, R., Nilsson, H., Ebihara, Y., Rème, H., Dandouras, I., Vallat, C., Bavassano-Cattaneo, M. B., Klecker, B., Korth, A., Kistler, L. M. and McCarthy, M.: Outflowing protons and heavy ions as a source for the sub-keV ring current, *Annales Geophysicae*, 27, pages 839-849, 2009.

Hoffman, J. H., Dodson, W. H., Lippincott, C. R. and Hammack, H. D.: Initial ion composition results from the Isis 2 satellite, *Journal of Geophysical Research*, Vol. 79, No. 28, pages 4246-4251, 1974.

Horwitz, J. L.: Core plasma in the magnetosphere, *Reviews of geophysics*, Vol. 25, No. 3, pages 579-587, 1987.

Hultqvist, B., Øieroset, M., Paschmann, G. and Treumann R.: Magnetospheric plasma sources and losses, *Space Science Reviews*, Vol. 88, Nos. 1-2, 1999.

Kaye, S. M., Shelley, E. G., Sharp, R. D. and Johnson, R. G.: Ion composition of zipper events, *Journal of geophysical research*, Vol. 86, No. A5, pages 3383-3388, 1981.

Klumpar, D. M.: Transversely accelerated ions: An ionospheric source of hot magnetospheric ions, *Journal of Geophysical Research*, Vol. 84, No. A8, pages 4229-4237, 1979.

Liszka, L.: The high-latitude trough in ionospheric electron content, *Journal of Atmospheric and Terrestrial Physics*, Vol. 29, pages 1243-1259, 1967.

Lundin, R., Lyons, L. R. and Pissarenko, N.: Observations of the ring current composition at  $L < 4$ , *Geophysical Research Letters*, Vol. 7, No. 6, pages 425-428, 1980.

Lundin, R., Eliasson, L., Haerendel, G., Boehm, M. and Holback B.: Large-scale auroral plasma density cavities observed by Freja, *Geophysical Research Letters*, Vol. 21, No. 17, pages 1903-1906, 1994.

Meng, C.-I.: Polar cap arcs and the plasma sheet, *Geophysical Research Letters*, Vol. 8, No. 3, pages 273-276, 1981.

Mizera, P. F. and Fennel, J. F.: Signatures of electric fields from high and low altitude particles distributions, *Geophysical Research Letters*, Vol. 4, No. 8, pages 311-314, 1977.

Moore, T. E.: Modulation of terrestrial ion escape flux composition (by low-altitude acceleration and charge exchange chemistry), *Journal of Geophysical Research*, Vol. 85, No. A5, pages 2011-2116, 1980.

Muldrew, D. B.: F-layer ionization troughs deduced from Alouette data, *Journal of Geophysical Research*, Vol. 70, No. 11, pages 2635-2650, 1965.

Murphree, J. S., Anger, C. D. and Cogger, L. L.: The instantaneous relationship between polar cap and oval auroras at times of northward interplanetary magnetic field, *Canadian Journal of Physics*, 60, pages 349-356, 1982.

Rème, H., *et al.*: First multispacecraft ion measurements in and near the Earth's magnetosphere with the identical Cluster ion spectrometry (CIS) experiment, *Annales Geophysicae*, 19, pages 1303-1354, 2001.

Sharp, R. D., Johnson, R. G. and Shelley, E. G.: Observations of an ionospheric acceleration mechanism producing energetic (keV) ions primarily normal to the geomagnetic field direction, *Journal of Geophysical Research*, Vol. 82, No. 22, pages 3324-3328, 1977.

Shelley, E. G., Johnson, R. G. and Sharp, R. D.: Satellite observations of energetic heavy ions during a geomagnetic storm, *Journal of Geophysical Research*, Vol. 77, No. 31, pages 6104-6110, 1972.

Shelley, E. G., Sharp, R. D. and Johnson, R. G.: Satellite observations of an ionospheric acceleration mechanism, *Geophysical Research Letters*, Vol. 3, No. 11, pages 654-656, 1976.

Tinsley, B. A.: Neutral atom precipitation – a review, *Journal of Atmospheric and Terrestrial Physics*, Vol. 43, No. 5/6, pages 617-632, 1981.

Ungstrup, E., Klumpar, D. M. and Heikkila, W. J.: Heating of ions to superthermal energies in the topside ionosphere by electrostatic ion cyclotron waves, *Journal of Geophysical Research*, Vol. 84, No. A8, pages 4289-4296, 1979.

Yau, A. W., Peterson, W. K. and Shelley, E. G.: Quantitative parametrization of energetic ionospheric ion outflow, in Moore, T. E. and Waite, Jr., J. H. (eds.) *Modeling magnetospheric plasma*, *Geophys. Monogr.* 44, 211, AGU, Washington, DC, 1988.

## Tables

<b>MLT sector</b>	<b><math>K_p \leq 2^-</math></b>	<b><math>2 \leq K_p \leq 4^-</math></b>	<b><math>K_p \geq 4</math></b>
Dawn	10	36	11
Noon	13	23	13
Dusk	4	21	9
Midnight	5	20	11

Table 1: Number of Cluster passages in the inner magnetosphere within each  $K_p$  bin.

<b>L</b>	<b><math>H^+ [cm^{-2} s^{-1}]</math></b>	<b><math>He^+ [cm^{-2} s^{-1}]</math></b>	<b><math>O^+ [cm^{-2} s^{-1}]</math></b>	<b>Passages</b>
$4.5 < L < 8.3$	$7.2 \cdot 10^6$	$1.2 \cdot 10^6$	$5.6 \cdot 10^6$	80
$4.5 < L < 12.1$	$6.4 \cdot 10^6$	$9.5 \cdot 10^5$	$4.5 \cdot 10^6$	166
$4.5 < L < 14.4$	$6.3 \cdot 10^6$	$9.3 \cdot 10^5$	$4.3 \cdot 10^6$	176

Table 2: Average fluxes of low-energy  $H^+$ ,  $He^+$  and  $O^+$  ions derived by removing outliers in  $L$  and number of Cluster passages within each specified  $L$ -value interval.

<b>MLT sector</b>	<b><i>L</i></b>	<b>Area</b> [cm <sup>2</sup> ]	<b>H<sup>+</sup></b> [cm <sup>-2</sup> s <sup>-1</sup> ]	<b>He<sup>+</sup></b> [cm <sup>-2</sup> s <sup>-1</sup> ]	<b>O<sup>+</sup></b> [cm <sup>-2</sup> s <sup>-1</sup> ]	<b>Passages</b>
Dawn	4.6 < <i>L</i> < 9.1	2.0 · 10 <sup>19</sup>	5.7 · 10 <sup>6</sup>	6.9 · 10 <sup>5</sup>	3.5 · 10 <sup>6</sup>	24
Noon	4.4 < <i>L</i> < 8.6	1.7 · 10 <sup>19</sup>	4.5 · 10 <sup>6</sup>	5.5 · 10 <sup>5</sup>	1.9 · 10 <sup>6</sup>	10
Dusk	4.5 < <i>L</i> < 8.5	1.7 · 10 <sup>19</sup>	7.5 · 10 <sup>6</sup>	2.1 · 10 <sup>6</sup>	8.6 · 10 <sup>6</sup>	22
Mid-night	4.4 < <i>L</i> < 7.4	1.1 · 10 <sup>19</sup>	9.5 · 10 <sup>6</sup>	1.1 · 10 <sup>6</sup>	6.5 · 10 <sup>6</sup>	24

Table 3: Average fluxes of low-energy H<sup>+</sup>, He<sup>+</sup> and O<sup>+</sup> ions. The right column shows number of Cluster passages within each specified L-value interval for each MLT sector.

<b>MLT sector</b>	<b>H<sup>+</sup> [s<sup>-1</sup>]</b>	<b>He<sup>+</sup> [s<sup>-1</sup>]</b>	<b>O<sup>+</sup> [s<sup>-1</sup>]</b>	<b>Passages</b>
Dawn	1.1 · 10 <sup>26</sup>	1.4 · 10 <sup>25</sup>	7.0 · 10 <sup>25</sup>	24
Noon	7.7 · 10 <sup>25</sup>	9.4 · 10 <sup>24</sup>	3.2 · 10 <sup>25</sup>	10
Dusk	1.3 · 10 <sup>26</sup>	3.6 · 10 <sup>25</sup>	1.5 · 10 <sup>26</sup>	22
Midnight	1.0 · 10 <sup>26</sup>	1.2 · 10 <sup>25</sup>	7.2 · 10 <sup>25</sup>	24
<b>Total outflow</b>	4.2 · 10 <sup>26</sup>	7.1 · 10 <sup>25</sup>	3.2 · 10 <sup>26</sup>	80

Table 4: Average outflows rates of low-energy H<sup>+</sup>, He<sup>+</sup> and O<sup>+</sup> ions. The right column shows number of Cluster passages within each MLT sector.

## Figures

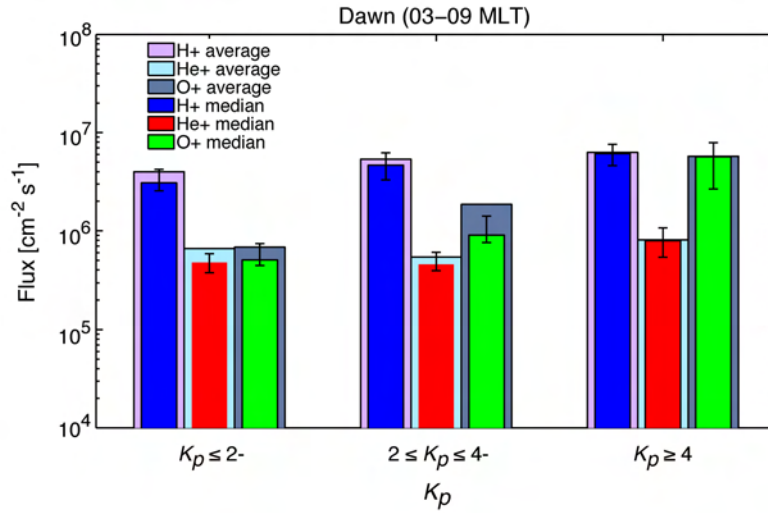


Figure 1: The narrow and broad bars represent the average and median flux of low-energy H<sup>+</sup>, He<sup>+</sup> and O<sup>+</sup> ions in the dawn sector (03:00 – 09:00 MLT) as a function of geomagnetic activity. This figure is based on data from 57 Cluster passages.

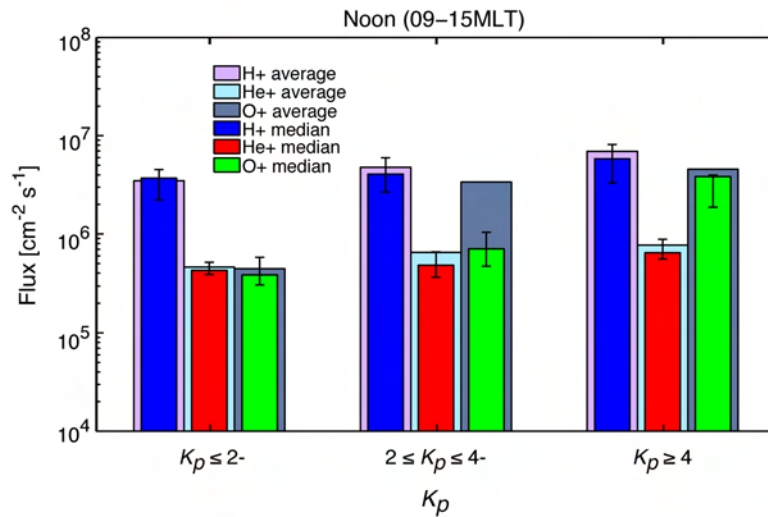


Figure 2: The narrow and broad bars represent the average and median flux of low-energy H<sup>+</sup>, He<sup>+</sup> and O<sup>+</sup> ions in the noon sector (09:00 – 15:00 MLT) as a function of geomagnetic activity. This figure is based on data from 49 Cluster passages.

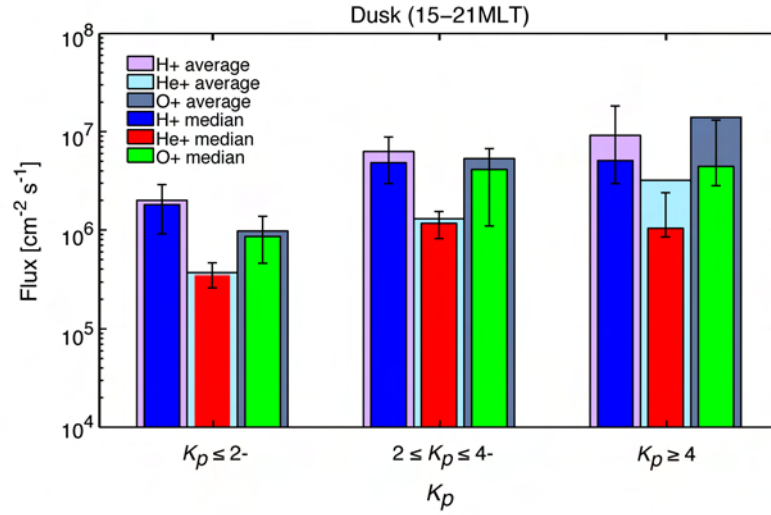


Figure 3: The narrow and broad bars represent the average and median flux of low-energy H<sup>+</sup>, He<sup>+</sup> and O<sup>+</sup> ions in the dusk sector (15:00 – 21:00 MLT) as a function of geomagnetic activity. This figure is based on data from 34 Cluster passages.

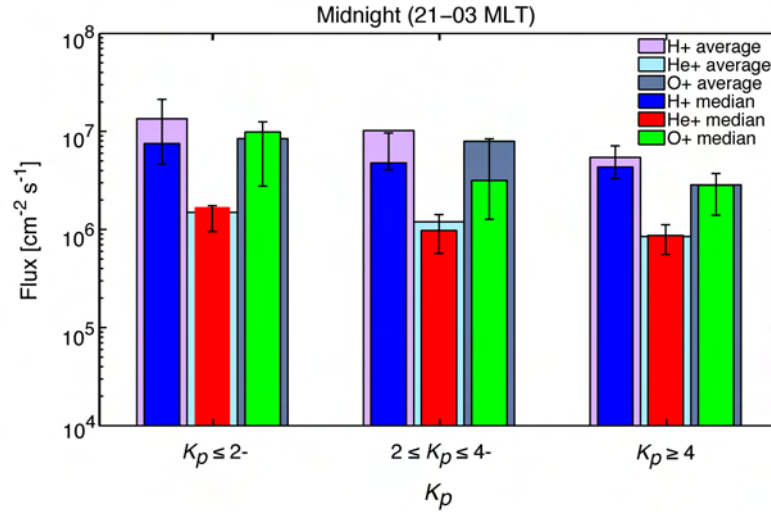


Figure 4: The narrow and broad bars represent the average and median flux of low-energy H<sup>+</sup>, He<sup>+</sup> and O<sup>+</sup> ions in the midnight sector (21:00 – 03:00 MLT) as a function of geomagnetic activity. This figure is based on data from 36 Cluster passages.



